ATMOSPHERIC SCIENCE

The efficiency of EURO 6d car particulate filters is compromised by atmospheric aging: In vitro toxicity of gasoline car exhaust

Mathilde N. Delaval[1]*, Hendryk Czech[1,2]*, Mohammad Almasaleekh[1,2], Svenja Offer[1,2], Jana Pantzke[1,2], Mika Ihalainen[3], Pasi Yli-Pirilä[3], Markus Somero[3], Miika Kortelainen[3], Nadine Gawlitta[1], Jürgen Orasche[1], Gert Jakobi[1], Deeksha Shukla[1,2], Patrick Martens[2,4], Andreas Paul[5], Zheng Fang[6], Michal Pardo[6], Alexandre Barth[7], Battist Utinger[7], Seongho Jeong[1,8], Narges Rastak[1], Evelyn Kuhn[1], Anja Huber[1], Arya Mukherjee[3], Arunas Mesceriakovas[3], Jorma Joutsensaari[9], Jani Leskinen[3], Anni Hartikainen[3], Johannes Passig[2], Sebastian Oeder[1], Jürgen Schnelle-Kreis[1], Thorsten Hohaus[5], Astrid Kiendler-Scharr[5]†, Markus Kalberer[7], Sebastiano Di Bucchianico[1,2], Yinon Rudich[6], Olli Sippula[3,10], Ralf Zimmermann[1,2]

Tailpipe emissions from road traffic contribute substantially to the burden of fine inhalable particulate matter ($PM_{2.5}$) and deteriorate air quality. Exhaust emission standards, forcing improvements in combustion and exhaust after-treatment technology, considerably decreases combustion-related $PM_{2.5}$ emitted by modern cars. A549 cancerous alveolar and BEAS-2B normal bronchial epithelial cells were exposed at the air-liquid interface to the total aerosol or gas phase of either fresh or photochemically aged tailpipe emissions from a gasoline EURO 6d car equipped with a gasoline particulate filter. Diluted fresh emissions contained particle number concentrations comparable to low ambient air levels and induced no detectable cytotoxicity. Photochemical aging led to the formation of secondary aerosols and caused significant cytotoxicity. While the aged aerosol induced significant DNA damage, oxidative stress was more associated with volatile secondary species. Our results call for the consideration of the exhaust emission atmospheric transformation processes in future emission standards toward health effect-driven emission regulations.

INTRODUCTION

Air pollution with elevated concentrations of fine inhalable particulate matter ($PM_{2.5}$), ozone (O_3), and nitrogen dioxide (NO_2) poses a global adverse threat for human health (*1*, *2*). Beyond evidence of significant effects on all-cause mortality, aggravated risks for respiratory diseases, cancer, and cardiovascular diseases have been identified for $PM_{2.5}$ and O_3 (*3*). The sources of air pollution cover a broad range from natural to anthropogenic emissions. They vary in toxicity and toxicological mechanisms, even at low concentrations (*4*). However, road traffic appears consistently in epidemiological studies as a substantial contributor to air pollution [traffic-related air pollution (TRAP)] and associated adverse health effects (*5*). This is also supported by experimental toxicological evidence (*6*–*8*). Several components (e.g., PM, NOx, and CO) in TRAP have already been included in current exhaust emission standards, e.g., EURO 6d in the European Union, Tier-3 in the United States, LEV-III in California, and China 6b in China. For a vehicle to receive certification, these regulated pollutants must not exceed upper limits of emissions per driven distance in a defined driving scenario, depending on the vehicle type.

Tailpipe emissions from light-duty gasoline vehicles have been identified as an important individual contributor to both gas and particle phase air pollutant levels (*9*, *10*). The introduction of gasoline direct injection (GDI) in spark ignition engines, replacing port fuel injection, improved fuel economy, thermal efficiency, and power output of gasoline vehicles, but shifted emissions from predominantly volatile organic compounds (VOCs) to higher PM levels (*11*). Gasoline particle filters (GPFs), adapted from diesel vehicles, have become a state-of-the-art tool in exhaust after-treatment technology to meet particle number (PN) concentration regulations and indirectly decrease primary emissions of air pollutants such as black carbon and polycyclic aromatic hydrocarbons (ArHCs). GPF often achieve filter efficiencies of >90% (*12*), potentially leading to reduced toxicity of exhaust emissions. However, no significant change in proinflammatory or oxidative stress-related biological end points in in vitro models has been observed when comparing unfiltered and filtered gasoline exhaust (*6*, *13*, *14*).

Reactions of aerosols in the atmosphere, commonly referred to as "aging," may increase ambient particle mass concentrations by oxidative gas-to-particle conversion accompanied by an increased average carbon oxidation state of the resulting organic aerosol (*15*, *16*). Recently, secondary organic aerosol (SOA), a major subfraction of $PM_{2.5}$, was associated with an increased risk of death from cardiorespiratory diseases in the United States (*17*). It is known that gasoline vehicles are major sources of SOA formation in urban

[1]Joint Mass Spectrometry Center (JMSC) at Comprehensive Molecular Analytics (CMA), Helmholtz Zentrum München, Neuherberg, Germany. [2]JMSC at Analytical Chemistry, Institute of Chemistry, University of Rostock, Rostock, Germany. [3]Department of Environmental and Biological Sciences, University of Eastern Finland, Kuopio, Finland. [4]Desert Research Institute, 2215 Raggio Parkway, Reno, NV 89512, USA. [5]Institute of Energy and Climate Research, IEK-8: Troposphere, Forschungszentrum Jülich GmbH, Jülich, Germany. [6]Department of Earth and Planetary Sciences, Weizmann Institute of Science, Rehovot, Israel. [7]Department of Environmental Sciences, University of Basel, Basel, Switzerland. [8]Institute of Chemical and Environmental Engineering, University of the Bundeswehr Munich, Neubiberg, Germany. [9]Department of Technical Physics, University of Eastern Finland, Kuopio, Finland. [10]Department of Chemistry, University of Eastern Finland, Joensuu, Finland.
*Corresponding author. Email: mathilde.delaval@helmholtz-munich.de (M.N.D.); hendryk.czech@uni-rostock.de (H.C.)
†Deceased.

areas, which is dominated by atmospheric oxidation of aromatic VOC emitted as unburned fuel or formed in the combustion process (*18*, *19*). Anthropogenic SOA from the photooxidation of naphthalene, as anthropogenic precursors, together with soot particles induced stronger biological responses in in vitro exposure studies compared to SOA from biogenic β-pinene as precursor (*20*–*22*), emphasizing the importance of aromaticity in emitted volatile hydrocarbons. In addition, lubrication oil makes a distinct contribution to primary organic aerosol (POA) emissions and may add to the overall aerosol toxicity (*23*, *24*).

The exposure of human bronchial epithelia to aged gasoline exhaust from EURO 5 vehicles exhibited significant cytotoxicity and impaired epithelial key-defense mechanisms when a versatile aerosol concentration enrichment system was used to enhance particle deposition from 13 to 342 ng cm^{-2} (*25*). A recent study investigated the impact of EURO 3 to EURO 5 gasoline vehicle emissions, both primary and aged, on cytotoxicity, intracellular generation of reactive oxygen species (ROS), and interleukin-6 (IL-6) as an indicator of proinflammatory response in human alveolar cells (*26*). However, differences in bioreactivity were small between primary and aged emissions of the same exhaust emission standard.

Emissions from modern gasoline vehicles, compliant with the current European exhaust emission standard EURO 6d, still lead to SOA formation exceeding the levels of POA (*27*, *28*). Moreover, no apparent difference in SOA formation between a EURO 5 light-duty gasoline vehicle, retrofitted with a GPF, and a EURO 6b gasoline car without GPF was observed (*28*, *29*). Therefore, the implementation of exhaust emission standards only partially succeeds in suppressing $PM_{2.5}$ from gasoline vehicles considering its combined primary and secondary origin.

In air quality standards, the effect of atmospheric processing on primary emissions of nitric oxide (NO) and VOC by regulating NO_2 and O_3 levels in ambient air is considered because of their established relevance to public health in epidemiological and toxicological studies (*30*, *31*). NO_2 predominantly originates from the oxidation of NO by O_3 and only to a minor extent from primary emissions, particularly from diesel engines (*32*). Furthermore, photochemical reactions of VOC by hydroxyl radicals (OH) in the presence of NO add to the burden of ground-level O_3 (*33*). In exhaust emission standards for on-road vehicles, the incorporation of NO by limits of NOx already anticipates its atmospheric conversion into the toxicologically more potent species NO_2 and further contribution to "photochemical smog." However, for emission limits of VOC, defined as hydrocarbons or "non-methane hydrocarbon (NMHC)," and $PM_{2.5}$ in ambient air, the connection is less stringent.

In the following, we reveal that extending this concept to precursors of secondary $PM_{2.5}$ is the next step to comply with ambient $PM_{2.5}$ regulations proposed by the World Health Organization (WHO) (*34*). We demonstrate that particle emissions from a gasoline light-duty vehicle with GPF and compliant with EURO 6d regulations, currently the strictest exhaust emission standard for light gasoline vehicles in the EU, are effectively reduced compared to previous emission exhaust standards. However, EURO 6d standard fails to cover emission conversion into secondary aerosols by photochemical aging upon atmospheric residence. We provide toxicological evidence that photochemical aging may toxify emissions from a EURO 6d gasoline car and discuss implications for public health.

RESULTS

Effect of aging on exhaust particles properties

Tailpipe emissions from a EURO 6d car, compliant with the currently strictest exhaust emission standard in the EU, EURO 6d, equipped with a GPF, were photochemically aged in a high-flow oxidation flow reactor (*35*). Because of the GPF, the number concentration of emitted particles was close to the scanning mobility particle sizer (SMPS) detection limit with an average of 200 particles per cm^3 in the diluted exhaust (Fig. 1A). In addition, only 3 μg m^{-3} of particulate organic matter (OM), could be detected by the aerosol mass spectrometer (AMS). Consequently, the content of ROS in the fresh exhaust particles and their oxidative potential (OP), determined by two complementary online techniques (online particle-bound ROS instrument, OPROSI and online OP ascorbic acid instrument, OOPAAI), were also below the limits of quantification of 0.01 nmol H_2O_2-eq. m^{-3} or equivalents of dehydroascorbic acid (DHA-eq.) m^{-3} (Fig. 1B).

Laboratory-aging using the oxidation flow reactor "PEAR" (*35*) with two equivalent days of photochemical aging raised the PN concentration to 6×10^7 per cm^3 with a PN median mobility diameter

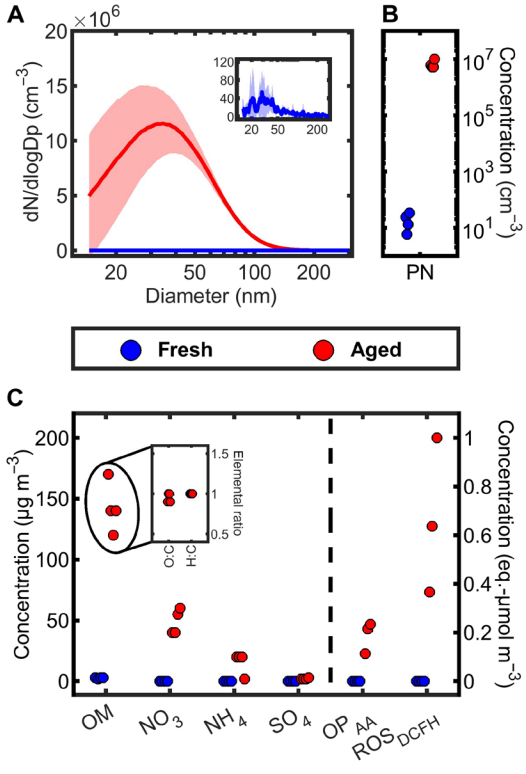

Fig. 1. PN concentrations and compositions in diluted tailpipe emissions. (**A**) PN size distributions and (**B**) total PN concentrations derived from SMPS. Shaded area denotes the SD of four experiments ($n = 4$). (**C**) Refractory particle components; OM, nitrate (NO_3), ammonium (NH_4), and sulfate (SO_4) from AMS, and two quantities representing oxidative particle properties from OOPAAI (OP_{AA}) in equivalents of dehydroascorbic acid (DHA-eq.) (*80*) and OPROSI (ROS_{DCFH}) in equivalents of H_2O_2 (*79*). ROS_{DCFH} and OP_{AA} could not be quantified in fresh exhaust particles due to concentrations below the limits of quantification. Insert in (C): Oxygen-to-carbon (O:C) and hydrogen-to-carbon ratio (H:C) in OM. Because of OM concentrations close to the limit of quantification, elemental ratio in fresh exhaust particles could not be determined.

of 35 ± 3 nm (Fig. 1A). Concurrently, after aging, OM, nitrate (NO_3), ammonium (NH_4) and sulfate (SO_4) increased respectively to average concentrations of 140, 49, 16, and 2 μg m^{-3} (Fig. 1C), indicating the formation of secondary PM from oxidative gas-to-particle conversion. However, considering the size distribution of the particles, only half of the particle mass was taken into account by the AMS measurement because of the dropping transmission efficiency for particles below 80 nm in the aerodynamic lens (*36*). Furthermore, atmospheric aging increases the OP and concentrations of ROS exerting biological effects in cell exposures (*37*, *38*). In contrast to undetectable ROS and OP in fresh aerosol particle emissions, OOPAAI and OPROSI analyses revealed OP_{AA} of 0.19 ± 0.06 μmol DHA m^{-3} and ROS_{DCFH} of 0.67 ± 0.32 μmol H_2O_2-eq. m^{-3}, respectively (Fig. 1C). Elemental ratios in the fresh exhaust particles could not be reliably determined because of low signal intensities for OM close to the limit of quantification. For particles in the aged exhaust, the average O:C and H:C were 1 (Fig. 1C), resulting in an average carbon oxidation state of 1, which is indicative of low volatility oxidized organic aerosol after an atmospheric residence time of few days (*39*). The measured particle effective densities were nearly constant as the function of particle size with an average density of 1.6 g cm^{-3}. Also, electron microscope images (fig. S4) indicate a compact morphology for organic-rich particles in the aged exhaust.

Effect of aging on gaseous exhaust components

Gaseous components in the exhaust passed a three-way catalyst, enhancing the yield of the complete hydrocarbon combustion products, carbon dioxide and water, and reducing nitric oxides (NO_x) to molecular nitrogen. The main gaseous product of incomplete combustion was carbon monoxide (CO) with an average concentration in the diluted exhaust of 12 parts per million (ppm), followed by ammonia (NH_3, 3.3 ppm), methane (CH_4, 1.0 ppm), and nitric monoxide (NO, 0.83 ppm); NMHCs, containing SOA precursors, accounted for 1.1 ppm (Fig. 2A). NO_2 (0.10 ppm) was less abundant than NO in the fresh exhaust but became the dominant NO_x species (= NO+NO_2) in the aged exhaust [NO: 0.78 parts per billion (ppb); NO_2: 5.3 ppb], but at significantly lower level than NO in fresh exhaust. Most of the primary NO_x was likely converted to nitrate species (gaseous HNO_3 and particulate nitrate), which are the main tropospheric sink of NO_x (*40*).

The sum of the volatile ArHCs in the fresh exhaust accounted for less than 5% of NMHC and was dominated by benzene followed by alkylated benzenes and naphthalene, which was shown by independent analyses with gas chromatography–mass spectrometry (GC-MS), proton-transfer-reaction (PTR), and resonance-enhanced multiphoton ionization (REMPI)–time-of-flight MS (TOFMS) (Fig. 2B) (*28*, *41*). Processing of the fresh exhaust in the PEAR (*35*) significantly decreased the concentrations of total ArHC (∑ArHC), but to different extents for individual ArHC according to their reactivity toward hydroxyl radicals (*42*). Consequently, the concentration of benzene was less affected by aging than alkylated benzenes or naphthalene (Fig. 2B); hence, benzene remained a major constituent also of the aged exhaust.

Of gaseous exhaust components accessible by PTR-TOFMS, ArHC had the highest concentration and accounted for 60% of all

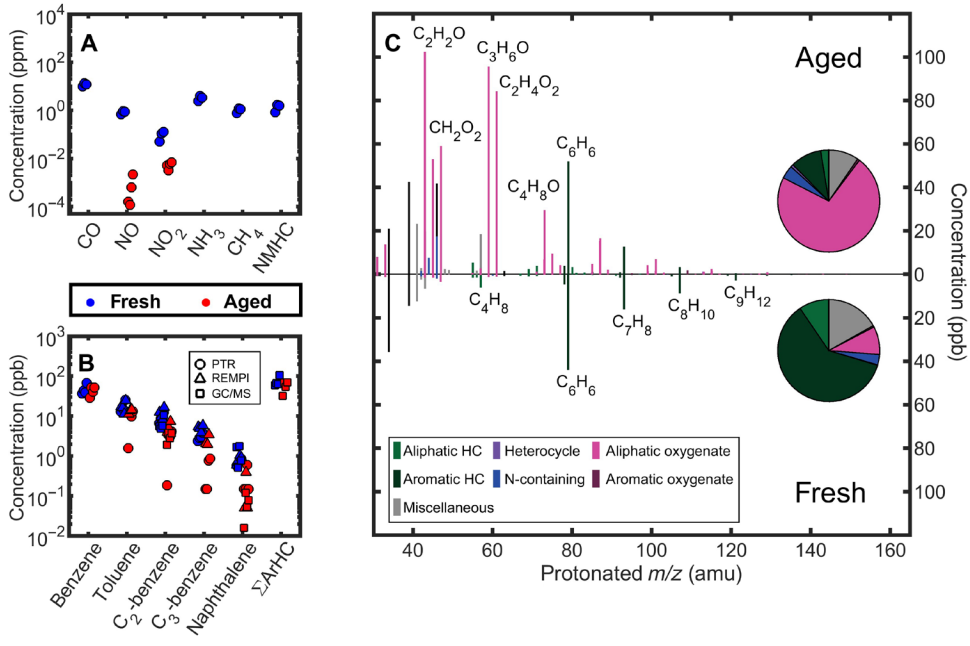

Fig. 2. Compositions and concentrations (in ppb v/v) of gases and VOCs in diluted car exhaust. (**A**) The concentration of carbon monoxide (CO), nitric oxide (NO), nitric dioxide (NO_2), ammonia (NH_3), methane (CH_4), and NMHCs in fresh exhaust derived by Fourier transform infrared spectroscopy; nitrogen oxides (NO + NO_2 = NOx) in the aged exhaust were measured by a chemiluminescence gas analyzer. (**B**) Concentrations of the five most abundant volatile ArHCs from PTR MS, REMPI MS, and GC-MS. Benzene and toluene could not be determined by offline sampling; hence, their concentrations from PTR measurements were added for total ArHC concentration (ΣArHC). (**C**) Representative PTR mass spectrum of the gas-phase composition. The sum formula refers to the composition of the VOCs in the exhaust, which are detected as protonated species. All quantities are corrected for a dilution of 17 used for the in vitro exposure experiments. PTR mass spectra of all experiments may be found in fig. S5.

detected VOCs. Oxygenated aliphatic, e.g., carbonyls and acids, with most abundant species having the sum formula C_2H_2O (ketene or oxygenate fragment), C_3H_6O (C3-carbonyl), and $C_2H_4O_2$ (acetic acid), dominated the volatiles in the aged exhaust (Fig. 2C). The increase in volatile carbonyl compound (CC) concentrations by aging is also supported by complementary selective sampling and quantitative analysis with isomeric resolution. The most abundant CCs in both fresh and aged emissions are the smallest CCs (formaldehyde, acetaldehyde, and acetone) that increased after aging by factors of 23, 4.9, and 2.8, respectively (table S5).

Effect of aging on the cytotoxicity of gasoline car exhaust emissions

Human alveolar A549 and bronchial BEAS-2B epithelial cells were exposed for 4 hours at the air-liquid interface (ALI) to fresh or photochemically aged aerosols from a EURO 6d gasoline car. Metabolic activity (Fig. 3A) and cell membrane damage (Fig. 3B) were evaluated after exposure by measuring the conversion of resazurin into resorufin by living cells and the cytosolic enzyme lactate dehydrogenase (LDH) release by dead cells. Primary (fresh) aerosols were not cytotoxic for both alveolar and bronchial epithelial cells compared to the negative controls [incubator (IC) and clean air (CA) controls]. However, photochemically aged aerosols caused a significant decrease of metabolic activity in alveolar (32% of IC) and bronchial epithelial cells (64% of IC). This decrease is also significantly different compared to the metabolic activity of cells exposed to fresh aerosol. Light microscopy observations indicated that cell detachment contributed to the decrease of metabolic activity after exposure to aged aerosol (not shown). This is confirmed by cell count of the remaining attached cells on inserts after exposure, with 75% (A549) and 48% (BEAS-2B) of detached cells, after exposure to aged aerosols, compared to IC (fig. S6). In addition, a significant increase of the LDH release, a marker of necrosis, was measured in both cell models (20% in A549 cells and 11% in BEAS-2B cells, i.e., 4.5- and 3-fold increase compared to the IC). Those results indicate an acute toxicity caused by aged aerosols by causing cell membrane damage, which could be due to the higher number of particles in the aged aerosols. On the basis of the PN concentrations derived from SMPS (Fig. 1), an estimated particle mass of 16 ± 3 ng cm^{-2} was deposited onto the lung epithelial cells exposed to photochemically aged aerosol compared to the very low estimated deposited particle mass (0.002 ± 0.004 ng cm^{-2}) for fresh aerosol exposed cells. However, exposure of the cells to gas phase (by filtration of the particles) showed that the aged gas phase was more toxic than the freshly emitted one and that it is the dominant cause for cell death. We observed a lower decrease of the cell number and of the metabolic activity for the cells exposed to the aged gas phase compared to the aged total aerosol (TA) (figs. S6 and S7).

Overall, the cytotoxic effect of the photochemically aged aerosol was more pronounced in the A549 cells (2-fold higher for metabolic activity and 1.5-fold higher for LDH release) compared to the BEAS-2B cells. This difference in sensitivity may be particularly relevant when considering our modeling results, which predict that, for aged emissions, approximately 69% of the total number deposition, 72% of the total surface area deposition, and 71% of the total mass deposition would occur in the alveolar region of the lungs—an area represented by the A549 cell line in our in vitro model (table S4).

Effect of aging on genotoxicity of gasoline car exhaust emissions

Results from the alkaline comet assay, which detects single and double DNA strand breaks as well as alkali labile sites such as apurinic or apyrimidinic sites, showed a slight (1.3-fold) but not significant ($P = 0.16$ for A549 and $P = 0.37$ for BEAS-2B) induction of DNA damage in lung epithelial cells exposed to fresh TAs in comparison to negative controls (Fig. 4, A and D). In addition, formamidopyrimidine DNA glycosylase (Fpg) and human 8-oxoguanine DNA glycosylase (hOGG1)–modified comet assays have been used for the measurement of oxidatively damaged DNA in lung epithelial cells. Fpg and hOGG1-modified versions of the assay revealed a generally higher level of oxidized DNA bases in both cell models exposed to either fresh or aged TAs (comprising both the particle and gas phases) compared to negative control samples (Fig. 4, B and C and E and F). In A549 and BEAS-2B cells exposed to aged TA, incubation with the Fpg enzyme uncovered 2.9 and 1.7 higher % DNA in tail, corresponding to 35- and 7-times higher amount of oxidized DNA bases, respectively, thus highlighting higher oxidative DNA damage in A549 with respect to BEAS-2B cells (Fig. 4, B to E). The levels of oxidative damage detected by hOGG1 enzyme increased up to 2.8 and 2.0% DNA in tail in the exposed A549 and BEAS-2B cells, respectively, representing 32- and 9-times increase compared to control cells (Fig. 4C). Filtration of particles reduced the oxidative DNA damage caused by aged emissions in both alveolar and bronchial cell models, with both enzymes. This reduction was only statistically

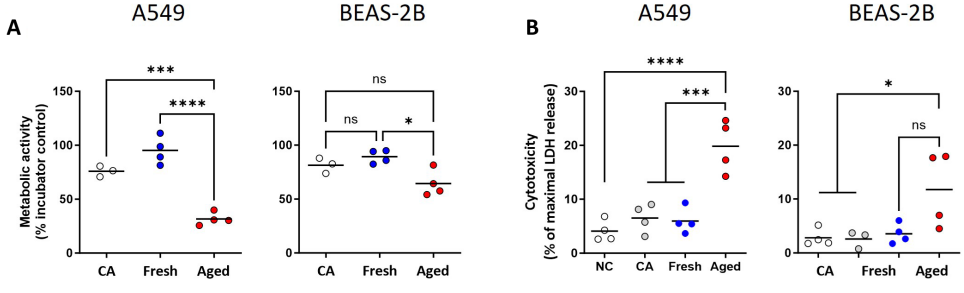

Fig. 3. Cytotoxic effects of fresh and aged gasoline car exhaust emissions on lung epithelial cells. Alveolar A549 and bronchial BEAS-2B epithelial cells were exposed at the ALI to 1:17 diluted fresh or aged gasoline car exhaust emissions for 4 hours. Directly after exposure, metabolic activity (**A**) was measured by the reduction of resazurin into resorufin, and cytotoxicity (**B**) was measured by the release of LDH. The metabolic activity and cytotoxicity of exposed cells is compared to cells exposed to CA or to cells left in the IC as negative controls. Results are presented as means ± s.e.m. One-way analysis of variance (ANOVA) with Tukey's post hoc test was used for multiple comparisons. *$P < 0.05$, ***$P < 0.001$, and ****$P < 0.0001$. ns, not significant.

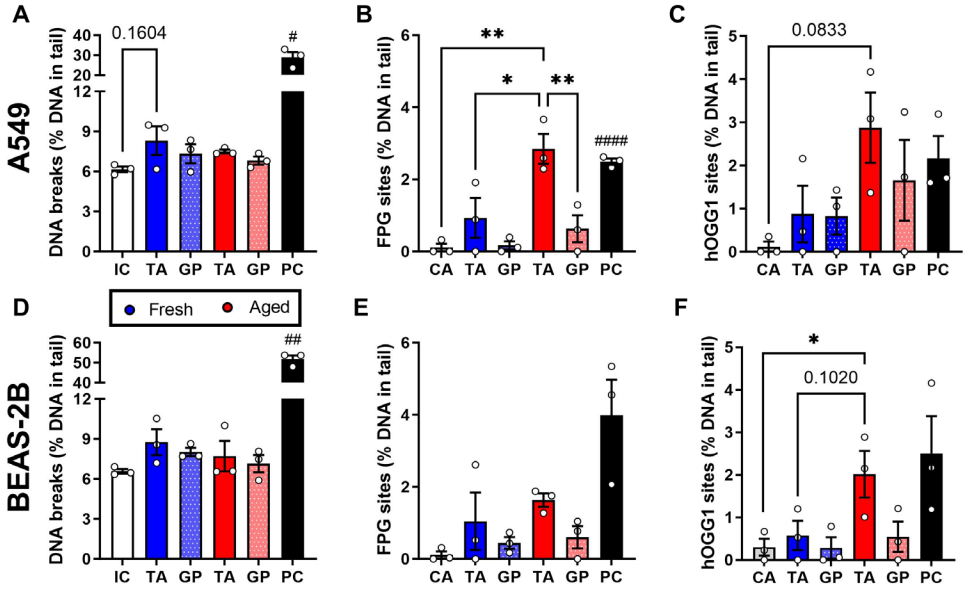

Fig. 4. DNA damage in lung epithelial cells induced by gasoline car exhaust emissions. Alveolar A549 (**A** to **C**) and bronchial BEAS-2B (**D** to **F**) epithelial cells were exposed at the ALI to total aerosol (TA) or gas phase (GP) of 1:17 diluted fresh or aged gasoline car exhaust emissions for 4 hours, and DNA damage was measured by Comet assay. DNA strand breaks were assessed by the alkaline version of the comet assay in A549 cells (A) and BEAS-2B cells (D). Positive controls (PC) = 50 μM H_2O_2. Incubator control, (IC). Oxidative DNA damage was detected in A549 (B and C) and BEAS-2B (E and F) cells with Fpg- and hOGG1-modified comet assay. Positive controls (PC) = 1.5 mM $KBrO_3$. Clean air, (CA). Bars represent means ± s.e.m. from three independent experiments. One-way ANOVA with Tukey's post hoc test was used for multiple comparison. *$P < 0.05$ and **$P < 0.01$. Unpaired *t* test was used for comparison of two conditions (NC versus PC, fresh versus aged, and TA versus GP). Statistical significance is then indicated by #.

significant in A549 cells with the Fpg version of the comet assay (fivefold decrease). This indicates the important contribution of the aged particulate phase to the oxidative DNA damage detected in exposed cells.

Proinflammatory and oxidative stress responses induced by fresh and aged aerosols of gasoline car exhaust emissions in lung epithelial cells

Proinflammatory and oxidative stress responses of alveolar and bronchial epithelial cells were assessed directly after exposure to fresh and photochemically aged aerosols emitted by EURO 6d gasoline car exhaust. Figure 5A displays the increase of the IL-8 release by alveolar A549 epithelial cells exposed to aged aerosol, compared to IC. However, there was no significant difference of IL-8 release between cells exposed to total aerosol and gas-phase only, although a trend is visible. The proinflammatory cytokine IL-6 was below the detection limit in exposure media from A549 cells. In bronchial BEAS-2B epithelial cells, exposure to fresh or aged aerosols induced no significant change in IL-8 or IL-6 levels (Fig. 5, B and C).

In addition, oxidative stress induction following exposure of lung epithelial cells to gasoline car exhaust emissions was evaluated by measuring the release of malondialdehyde (MDA), a marker of lipid peroxidation, in cell exposure medium and the oxidized glutathione (GSSG)/reduced glutathione (GSH) ratio in cells. MDA release increased by 10 and 4 times in cell culture medium from A549 and BEAS-2B cells exposed to photochemical aged aerosols, respectively, with no difference between total aerosol and gas-phase exposed cells. There was no change in MDA release from cells exposed to fresh aerosol, compared to negative controls (Fig. 5D). No significant change in the intracellular glutathione oxidation level was observed in both cell models exposed to fresh or aged aerosols (Fig. 5, E and F).

DISCUSSION

Our study examined the toxicological impacts of tailpipe emissions from a EURO 6d GDI gasoline light-duty vehicle equipped with a GPF and secondary aerosols formed from photochemical aging of the vehicle exhaust in a high-flow oxidation flow reactor. Alveolar and bronchial epithelial cells were exposed at the ALI to either diluted fresh or photochemically aged aerosols, while both chemical and physical aerosol properties were thoroughly characterized for investigating the relation between biological responses and aerosol properties.

To our knowledge, this is the first study to demonstrate the toxicity of photochemically aged exhaust emissions from a gasoline EURO 6d car with GPF by using a methodology mimicking realistic exposure conditions (*43*, *44*), which we already successfully used for assessing the impact of soot particles coating with SOA toxicity (*20*, *21*). We combined the ALI cell exposure method with the aerosol photochemical ageing process, which markedly affects the composition and health impacts of atmospheric pollutants (*45*). Furthermore, the ALI exposure allows for the physicochemical characteristics of both gas and particle phases of the aerosol to not be affected by the components of the cell culture medium (*46*). The A549 and BEAS-2B cell lines used in this study represent the epithelial cells lining the alveolar and bronchial regions in the lungs. These cells are widely used in inhalation toxicology as they are sensitive to detect cellular and molecular toxic effects at low environmental doses, similar to human exposure for particles (*20*, *47*, *48*) and gaseous compounds (*49*–*51*).

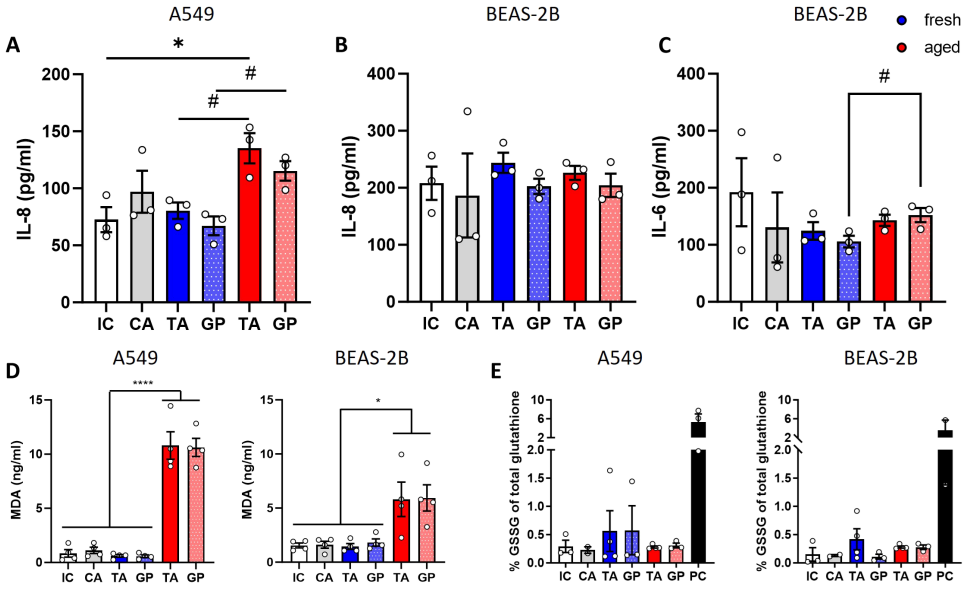

Fig. 5. Proinflammatory and oxidative stress responses induced by gasoline car exhaust emissions in lung epithelial cells. Alveolar A549 and bronchial BEAS-2B cells were exposed to the ALI to total aerosol (TA) or gas-phase (GP) of 1:17 diluted fresh or aged gasoline car exhaust for 4 hours. After exposure, basolateral medium from the exposed cells were collected for later measurements. IL-8 and IL-6 cytokine release was measured by enzyme-based immunosorbent assay (**A** to **C**). MDA release was measured by LC-MS/MS (**D**). Cells were collected, and the ratio of GSSG/GSH was measured by LC-MS and compared to negative controls, PC: 100 μM menadione (**E**). Bars represent means ± s.e.m. from three or four independent experiments. One-way ANOVA with Tukey's post hoc test was used for multiple comparison. *$P < 0.05$ and ****$P < 0.0001$. Unpaired *t* test was used for comparison of two conditions (NC versus PC, fresh versus aged, and TA versus GP). Statistical significance is then indicated by #.

Our study primarily revealed that photochemically aged emissions from gasoline car exhaust caused acute biological effects after short exposure of lung epithelial cells, as observed by increased cytotoxicity, as well as genotoxicity, proinflammatory response, and oxidative stress induction. In addition, we found that diluted tailpipe particle levels were very low because of the installation of the GPF at the car exhaust pipe, complying with air quality regulations. The efficient removal of particles, which are well known for their toxic potential (*52*), could explain the noncytotoxic effect of the fresh aerosol on lung epithelial cells. Furthermore, our study revealed that photochemical aging leads to a considerable formation of secondary PM from oxidative gas-to-particle conversion involving VOC and NO_x with NH_3 as alkaline counterpart for the acidic oxidized vapors. The increased toxicity induced by aged aerosol in lung epithelial cells could be related to the presence of newly formed particles during photochemical ageing. Filtering the aerosol directly in front of the cell exposure setup did not significantly reduce the induced cytotoxicity, proinflammatory response, or oxidative stress in both lung models. Only oxidative DNA damage caused by the aged aerosol was significantly reduced by the filtration of particles. These results suggest that while the gaseous components of the aerosol mainly drive the toxicity of both primary and secondary gasoline car exhaust emissions, the particulate phase also contributes to the toxicological impacts of car exhaust emissions. This raises concern on the long-term effects of gasoline car exhaust on human health despite the use of GPF. However, it has been demonstrated that SOA from moderately aged aromatic precursors is largely semi-volatile (*20*, *39*). Therefore, it is plausible that PM first retained in the filter may continuously revolatilize in the exhaust flow and reach the cell models as gas phase species.

In human airways, the deposition of PM is expected to be higher in the alveolar region than in the bronchial regions (*53*). Our estimation of International Commission on Radiological Protection (ICRP) model–based lung deposition of the aged exhaust particles also supported this conclusion. Together, PM deposition can potentially lead to a significant impairment of the alveoli, especially considering the observed increase of IL-8 by alveolar cells but not by bronchial cells.

Aged aerosol induced a significant release of IL-8, an oxidative stress–responsive proinflammatory chemokine, in A549 but not BEAS-2B cells. IL-8 is a potent chemoattractant released from epithelial cells following particle-induced oxidative stress (*54*), and its release can lead to neutrophil influx and inflammation in the lungs (*55*). Inflammatory processes also increase the production of free radicals in lungs and defense cells, which could in turn enhance oxidative stress. We also found that total aged gasoline EURO 6d car exhaust increased the oxidative DNA damage and lipid peroxidation (MDA release) in both alveolar and bronchial epithelial cells, although no intracellular oxidative stress was detected with the glutathione assay. Lipid peroxidation indicates that aged aerosol caused oxidative damage to the cellular membranes and other cell components containing lipids. This could be related to the OP of the particles in aged aerosol as measured with online ROS and OP measurements (Fig. 1C). Aerosol particles can initiate the production of ROS in cells, inducing oxidative stress and further causing damage to cellular structures, including DNA, proteins, and lipids. Previous in vitro studies demonstrated that SOA produced from photochemical aging of naphthalene and trimethylbenzene, both representative anthropogenic SOA precursors, induces oxidative stress in different in vitro lung models (*20*, *21*, *37*, *56*).

We found that short exposure to photochemically aged aerosol from gasoline EURO 6d car exhaust induced genotoxic effects in lung epithelial cells. This is concordant with several studies that previously addressed the potential of fuel exhaust emissions to damage genetic material in human airways (*57*) and detected chromosomal and DNA damage in human bronchial and alveolar epithelial cells exposed to emissions from diesel or gasoline engines (*13*, *58*–*60*). On the other hand, Usemann *et al.* (*13*) showed that the use of GPF reduced oxidative DNA damage in bronchial epithelial cells after whole gasoline car (EURO 5) exhaust exposure. This finding contradicts our findings that both fresh and aged aerosols led to slight DNA damage and significant oxidative DNA damage in lung epithelial cells. DNA damage, that is, at least in part, caused by oxidative stress, has been typically involved in the molecular pathogenesis of chronic inflammatory airway diseases by inducing apoptosis, cell senescence, and proinflammatory responses (*61*, *62*).

There are some limitations to the present study, including the cell models, the unique dose of exposure, as well as car operation and laboratory aging. The two cell lines used in this study, although widely used in inhalation toxicology, present differences with the in vivo situation, e.g., they do not form tight junctions, one of the key features of epithelial barriers functions (*63*). Human airways are formed of a functional tight epithelial layer, comprising more than 40 known cell population types, including immune cells and fibroblasts, which play a crucial role in the inflammation caused by airborne pollutants in the lungs and in the development or exacerbation of lung diseases (*64*, *65*). By increasing the complexity and physiological relevance of the cell models, their predictivity can then be improved for more accurate human risk assessment (*43*). For instance, the use of more complex lung epithelial models, such as primary human airway epithelia (*25*) or coculture lung cell models comprising immune-competent cells (*66*), could provide valuable information on the cellular cross-talk, immune responses, and more physiologically relevant toxicological outcomes of the human airways in response to EURO 6d car exhaust emissions. Because of the limited biological assays used for evaluating the toxicological effects caused by atmospheric aging in model vehicles, we can only hypothesize the underlying mechanisms of toxicity. Signaling pathways should be further explored to better understand the mechanisms of toxicity of the gasoline exhaust emissions and especially to decipher the relation between the aerosol chemical components and their toxic potential (*25*). Eventually, our results should be interpreted as part of a broader risk assessment framework that incorporates additional in vitro, in vivo, and clinical evidence. While in vitro models provide critical mechanistic insights into cellular responses, translating these results to human exposure requires consideration of realistic exposure doses, deposition patterns, and advanced approaches such as in vitro–to–in vivo extrapolation, which account for physiological and dosimetric differences between cell models and the human respiratory system (*67*).

The toxicity of car exhaust can vary depending on factors such as driving conditions, engine performance, fuel quality, and the specific emissions control technologies used by modifying the chemical composition and physical properties of the generated emissions (*9*, *68*). The specific toxicity of the aerosols generated during the different cycle speeds should be evaluated in future studies. This could provide indication on behavioral driving conditions for reducing car emissions, for complementing the current emission limits. Engine operation conditions were found to notably affect the exhaust composition and secondary aerosol formation potential (*29*), although Lau *et al.* (*26*) found small or insignificant difference of toxicity of primary and aged emissions of EURO 3 to 5 regulation car run under different driving conditions in A549 cells.

Gasoline vehicle emissions from real driving are highly dynamic and cover different concentration and composition regimes. To enable comparability of vehicle emissions on dynamometers, standardized protocols, such as the Worldwide Harmonized Light Vehicles Test Procedure (WLTP), have been established. The driving cycle in this study involves less dynamic driving, presumably leading to lower emissions than in the WLTP. However, this simplification of the driving cycle does not affect the general conclusion of this study as the increase in secondary PM after photochemical aging and associated cell responses in several biological endpoints are highly significant.

Laboratory aging of gasoline car emissions were conducted with the PEAR as a model to study photooxidation chemistry (*35*). The residence time in the PEAR was only 70 s; thus, some of the oxidized vapor–phase compounds may have insufficient time to condense as aerosol particles and leave the PEAR in the GP. In addition, oxidized vapors formed secondary PM in the ultrafine range by nucleation instead of condensing on primary particles because the external condensation sink of the fresh tailpipe emissions was removed by the GPF. Although the OFR (oxidation flow reactor) conditions can be principally adjusted to simulate OH-dominated reactions similar to ambient tropospheric air (*69*), our experimental conditions deviate from that regarding non-OH fate of VOC, NO_x, and RO_2 radical chemistry (*70*, *71*). Nevertheless, the bulk composition of the secondary PM, the relevance of ArHC for the formation of SOA, and the substantial formation of NH_4NO_3 triggered by high NH_3 emissions are similar to a chamber experiment with another EURO 6 gasoline car without GPF, with the same fuel and similar ageing equivalent to 1.5 days (*29*). Because of the high-average carbon oxidation state and ammonium nitrate content, and absence of solid PM after the GPF, the secondary PM is assumed to dissolve instantaneously when deposited on the cells. Consequently, the sizes of the particle play a minor role for the observed biological effects.

Together, we observed substantial secondary particle formation by photochemical aging of tailpipe emissions from a light-duty gasoline vehicle with GPF, which is considered "clean" and represents the current available state-of-the-art emission reduction technology. In addition, our study reveals the role of gaseous exhaust components in the significant increase of toxicity of the emissions from the gasoline EURO 6d car exhaust by photochemical aging. Therefore, our results call for the rethinking of emission exhaust regulations and the development of protocols for a standardized consideration of atmospheric processes. Future regulations can be imposed for example by speciation of ArHC in tailpipe emissions in dynamometer tests because ArHC are the most potent class and toxic of SOA precursors. Such anticipation of the atmospheric fate of primary volatile emissions from the transport sector, such as illustrated by NO and NO_2, may substantially support measures for compliances with the revised EU Directive 2008/50/EC of maximum annual mean $PM_{2.5}$ values of 20 $\mu g\ m^3$ and toward WHO guidelines of 5 $\mu g\ m^{-3}$.

MATERIALS AND METHODS

Tailpipe emissions from a light-duty gasoline car: Test vehicle, fuel, test cycle and sampling

Experiments were conducted at the ILMARI facility of the University of Eastern Finland with a turbocharged light-duty GDI passenger vehicle (Skoda Scala 1.0 TSI, model year 2021, further details in table S1, and experimental setup in fig. S1) on a chassis dynamometer (Rototest VPA-RX3 2WD). For exhaust after-treatment, the car was equipped with a three-way catalyst and a GPF, compliant with EURO 6d exhaust emission standard. The car was operated with commercial gasoline-ethanol blend fuel 95 E10 (gasoline with max. 10% ethanol content) according to a four-times repeated driving cycle with following conditions: cold start and idling for 5 min (no gear), 50 km hour^{-1} for 15 min (4th gear), 100 km hour^{-1} for 15 min (5th gear), 80 km hour^{-1} for 15 min (5th gear), and idling for 5 min (no gear). This procedure was repeated four times for a total experimental duration of 4 hours, while for the second to fourth repetitions, the cold start was replaced by a hot start. The wheel power was chosen to represent the wheel and air frictions of the vehicle at the given speed.

A partial flow from the vehicle exhaust was sampled and diluted in a combination of porous tube diluter and ejector diluter. The dilution ratio was defined by measuring the CO_2 concentrations before and after the dilution process. The dilution ratio was controlled by the flow rate in the porous tube diluter, while the ejector diluter flow rate remained constant. The total dilution ratio was set to 17, and the control process was automated. The sampling line before the diluters was heated to 120°C. An example of gaseous emissions over one 4-hour experiment and engine conditions is depicted in fig. S2.

Photochemical aging in oxidation flow reactor

The oxidation flow reactor PEAR (*35*) was used for simulating atmospheric aging of tailpipe emissions in about 1 min of processing in the laboratory. The PEAR consists of a stainless steel cylinder with a total volume of 139 liter and contains four adjustable ultraviolet (UV) lamps (Osram, HNS 55W G13 HO; main emission at 254 nm, blocked emission at 185 nm). The main design features of the PEAR are large volume for high flow rates, the design of the diffuser at the beginning of the reactor to reduce undesired back flows, and stainless steel construction to avoid losses of charged particles.

Diluted tailpipe emissions were premixed with O_3 and water vapor to achieve 7 ppm of O_3 and a minimum relative humidity (RH) at room temperature of 40% (humidifier model 125-240-5MP; Perma Pure ltd., USA), controlled by a photometric ozone analyzer (model 49i Ozone Analyzer, Thermo Fisher Scientific Inc., MA, USA) and humidity sensor (HMP 110/65, Vaisala, Finland). A total flow rate of 120 liter min^{-1} determines the mean residence time to 70 s, while the most abundant residence time is expected to be shorter (*35*). Using four UV lamps at 8 V, a total photon flux of $9.42 \cdot 10^{15}$ photons cm^{-2} s^{-1} was generated, initiating the formation of hydroxyl radicals from O_3 photolysis and subsequent reaction of the singulet oxygen $O(^1D)$ with water vapor according to

$$O_3 + h\nu(254nm) \rightarrow O_2 + O(^1D)$$

$$H_2O + O(^1D) \rightarrow 2 \times OH$$

The OH exposure, i.e., the equivalent photochemical age, was experimentally determined by adding isotope-labeled butanol (D9-BuOH, 98% isotopic purity; Sigma-Aldrich) with a concentration of approximately 100 ppb in an experiment without cell exposure. D9-BuOH reacts with non-OH oxidants to a negligible extent and is therefore a valid "photochemical clock" (*72*). From the decay of D9-BuOH inside the PEAR, measured by a PTR-TOFMS (Ionicon Inc., Vienna, Austria), and a rate constant k_{OH} of 3.4×10^{-11} s cm^{-3}, the OH exposure was determined every 10 s. For the entire experiment, the harmonic mean accounts for 2 days of equivalent photochemical aging, assuming an average ambient ·OH concentration of 1.5×10^6 molec cm^{-3}. Before offline sampling of VOC and PM on adsorbent tubes and quartz fiber filters as well as cell exposure, the aged exhaust passed ozone denuders. The ozone denuders consist of ceramic honeycombs, which were impregnated with potassium nitrite (KNO_2) and decomposed ozone according to

$$KNO_2 + O_3 \rightarrow KNO_3 + O_2$$

Assessment of aging OFR conditions

The importance of the non-OH radical fate of VOC was assessed using the Oxidation Flow Reactor Exposure Estimator (v3.1) for OFR (*70*, *71*, *73*, *74*) using data from Fourier transform infrared (FTIR) gas analysis and ozone monitoring as input. The temporal evolution of NMHCs and NO_x ($NO+NO_2$) as well as external OH reactivity (OHR_{ext}) over the driving cycle was highly dynamic including changing NMHC/(NMHC+NO_x) (fig. S2). On the one hand, NO_x, primarily released as NO partly consumes externally fed ozone, which is not available anymore for the generation of OH radicals. On the other hand, water vapor in the emissions increased the RH inside the PEAR, which may be up to 64% depending on engine condition and stimulate the OH radical production. Overall, the used OFR conditions are in the transition space of atmospherically relevant ratio of photon flux at 254 nm and OH exposure, apart from cold engine start and the beginning of a new driving cycle where the system departs from the atmospheric relevant region for a period shorter than the mean PEAR residence of 70 s (*75*). Consequently, photolysis at 254 nm may even dominate the degradation of ArHC, particularly for benzene. However, this only occurs during the first 15 min of each cycle when NMHC/(NMHC+NO_x) approaches minimum values around 0.2; hence, a minority of the total aged aerosol leaving the PEAR was affected by photolysis (*76*). The fate of RO_2 radicals in the PEAR affects the individual product formation in SOA, which was assessed using the model from (*71*). In all experiments, the RO_2 fate was dominated by the reactions with the hydroperoxyl radical (RO_2+HO_2) from 91.2 to 93.4%. The second most important pathway was the reaction with hydroxyl radicals (RO_2 + OH; 6.2 to 8.6 %), which has a negligible relevance in ambient air. Minor contributions from RO_2 reaction were obtained with NO (0.1 to 0.2 %), other RO_2 radicals (RO_2 + RO_2; <0.01 %), or isomerization of RO_2 (0.1 %), which were underrepresented compared to ambient air (*76*). Despite giving insights into the OFR gas phase chemistry and reaction conditions, the composition of SOA may not substantially deviate from smog chamber studies with oxidation conditions closer to atmospheric processes or between OFR-generated SOA of differently modeled atmospheric relevance (*77*).

Instrumentation for physical and chemical analysis of the particle phase

PN and particle size distributions in diluted primary and aged aerosol emissions were evaluated using an SMPS [consisting of a condensation particle counter (CPC, TSI Model 3775low, USA), and a differential mobility analyzer (DMA, TSI Model 3082, USA)]. OM,

particulate nitrate (NO_3), ammonium (NH_4), and sulfate (SO_4) were measured with a high-resolution TOF AMS (Aerodyne Inc., Billerica, MA, USA), while elemental ratios of AMS-derived OM were determined by the "improved-ambient" method (*78*). Additional dilution for AMS measurements of the aged aerosol emissions was provided by an ejector diluter with a fixed dilution of approximately 8 (Dekati Ltd., Finland). Measurements of oxidative particle properties were conducted using the OPROSI based on a chemical assay of 2′,7′-dichlorofluorescein (DCFH) with horseradish peroxidase and fluorescence spectroscopic detection measured as ROS_{DCFH} (*79*) and OOPAAI using ascorbic acid as antioxidant measured as OP_{AA} (*80*, *81*). The samples for electron microscopy [scanning electron microscopy (SEM) and transmission electron microscopy (TEM)] were collected on holey carbon substrates with copper supported grids (Agar Scientific, S147-4, UK) using an aspiration sampler (*82*). Particles were separately collected for all velocity phases in a driving cycle. The single particle morphology was analyzed using a field-emission SEM (Sigma HD, Zeiss, 0.02-30 kV, D) and a field-emission TEM (JEM-2100F, JEOL, 200 kV, JPN). Last, the particle effective densities for different driving conditions were measured by a setup consisting of an Aerosol Particle Mass Analyzer (APM 3600, Kanomax, USA) and an SMPS (CPC 3776 and DMA 3081, TSI, USA) following the methodology described by Leskinen *et al.* (*83*).

Instrumentation for analysis of the gas phase

Fresh gaseous emissions were analyzed without dilution by an FTIR multicomponent gas analyzer (model DX4000, Gasmet Oy, Vanta, Finland), including inorganic gases CO, CO_2, water vapor, NO_x ($NO+NO_2$), and NH_3 as well as 30 volatile hydrocarbons, aromatics, and oxygenates from methane to C_9 species. Calibration of the FTIR was performed externally with gas standards. Furthermore, NO and NO_2 were measured after PEAR by a NO_x gas analyzer based on chemiluminescence (42i NO-NO_2-NOx Analyzer; Thermo Fisher Scientific Inc., MA, USA). The organic composition of the gas phase was monitored by a PTR-TOFMS (PTR-ToFMS 8000, Ionicon Analytik, Innsbruck, Austria) (*84*), operated with H_3O^+ as the primary ion and in the mass/charge ratio (m/z) range of 10 to 500, with a time resolution of 10 s and a mass resolution $m/\Delta m$ of 5000 (full width at half maximum at m/z 79) at the mass of protonated acetone. Semiquantification was conducted according to (*85*). The PTR-TOFMS alternately analyzed diluted fresh or aged emissions. For selective analysis of aromatic VOCs, an REMPI-TOFMS (PHOTO-TOF-MS, Photonion GmbH, Germany) was used. UV radiation of 266 nm (fourth harmonic generation) was provided by an Nd:YAG laser (Big Sky Ultra; Quantel, France; 20-Hz repetition rate, 1064-nm fundamental radiation, and energy of 2 mJ at 266 nm). At 266 nm, preferably ArHC are detected in vehicle exhaust emissions. Quantification was based on the method of ionization cross sections of individual analytes relative to toluene (*86*), which was continuously added as isotope-labeled toluene (m/z 95; toluene methyl-D3, 98% isotopic purity, Cambridge Isotope Laboratories Inc., MA, USA) (*87*) with a concentration of approximately 400 ppb; the true concentration was determined by comparison with a 1-ppm toluene gas standard (Linde AG, Germany).

Gas phase samples for offline analysis were collected with adsorbent tubes consisting of three sublayers of graphitized carbon black sorbents to trap VOC and IVOC (table S2) for 4 hours at a flow rate of 0.9 liter min^{-1}. Quartz fiber filters were installed in front of the adsorbent tubes to remove particles. Samples and field blanks were stored at −20°C until analysis. The analysis of the gas phase adsorbers was performed on by GC-MS (Shimadzu GCMS-QP2010 Ultra, Shimadzu, Japan) equipped with a thermal desorption unit (Shimadzu TD-20, Shimadzu, Japan). Thermal desorption was performed at 345°C for 45 min. Desorbed compounds recondensed and concentrated on a Tenax TD trap at 5°C from which they were redesorbed at 330°C and transferred to the GC at a split ratio of 30. A VF-xMS, high arylene modified phase column (30 m + 5 m precolumn, 0.25-mm ID by 0.25-μm d_f, Agilent Varian, USA), was used. GC oven temperature was 60°C for 6 min and increased to 250°C at a temperature rate of 5°C/min. Column flow was 1.6 ml/min, and total analysis time was 44 min. The MS was operated with an ion source temperature of 230°C, an interface temperature of 250°C, and in scan mode with a solvent cut time of 2 min and a scan speed of 1666 amu/s in the m/z range of 35 to 500. An isotope-labeled standard mixture was applied to the sample before analysis (table S3). Equivalent target compounds and similar target groups were quantified according to the respective standard compound summarized in table S3.

Reactive sampling of CCs was conducted from the main engine stack over a 240-min interval, using a dilution ratio of 17 and using a sampling flow of 0.216 m3. The sampling methodology involved the utilization of DNPH cartridges "ORBO/54020-U" provided by Sigma-Aldrich (Germany) with high sample volume capacity. The cartridges were packed with a dual-bed DNPH (2,4-dinitrophenylhydrazine) sorbent supported on silica gel. The initial bed encompassed 300 mg of DNPH in the front section and 150 mg in the rear section and was used for the analyses. Upon completion of the sampling procedure, the cartridges were promptly disengaged from the sampling line, sealed with polytetrafluoroethylene (PTFE) caps, and stored at a temperature of −20°C until subjected to subsequent analysis. CC-hydrazones were finally quantified by high-performance liquid chromatography (HPLC) coupled with diode array detection (Agilent 1260 Infinity II, USA). The main bed was extracted with 1 ml of acetonitrile (ACN), and then a 10-μl aliquot was injected into the HPLC system through an autosampler. A C18 LC column (4.6 mm by 150 mm, Eclipse Plus C18; Agilent, USA) at 40°C with gradient mobile phase configuration was used, commencing with 60% ACN and 40% deionized (DI) water at the onset (0 min), which was gradually adjusted to reach 100% ACN and 0% DI water over a span of 9 min. Subsequently, a 6-min flushing with 100% ACN was executed, followed by a return to the initial conditions of 60/40% ACN/DI water. The mobile phase was maintained at a flow rate of 1 ml/min. Detection was carried out using a UV detector set at 360 nm.

Cell culture

A549 [American Type Culture Collection (ATCC) CCL-185] and BEAS-2B (ATCC, CRL 9609) human lung cell lines were used in our study as they are commonly used as model cells in respiratory toxicology and are representative of the alveolar and bronchial regions on the human airways. A549 cells are alveolar type II carcinoma cells, while BEAS-2B are SV-40–transformed normal bronchial epithelial cells.

A549 cells were routinely cultured in high-glucose Gibco Dulbecco's modified Eagle medium: nutrient mixture F-12 (DMEM/F-12) (Thermo Fisher Scientific, 31331-028, USA) supplemented with 5 % (v/v) fetal bovine serum (FBS) (Thermo Fisher Scientific, 10500-064), penicillin (100 U ml^{-1}), and streptomycin (100 μg ml^{-1}) (Sigma-Aldrich, P4333) in a humidified incubator at 37°C and 5 % carbon dioxide (CO_2). A549

cells were seeded on transferrable 24-mm Transwell inserts with a polyester membrane (0.4-μm pore size; six-well plate format, Corning, #3450) 48 hours before the exposure experiments at a density of 3×10^5 cells per insert (6.5×10^4 cells cm^{-2} growth area) in 1 ml of cell culture medium in the apical compartment and 1.5 ml in the basolateral compartment of the Transwell inserts. Twenty-four hours after seeding, the culture medium on the apical side was removed to establish ALI conditions.

BEAS-2B cells were cultured with BEBM Bronchial Epithelial Cell Growth Basal Medium (Lonza, CC3171) supplemented with the recommended BEGM Bronchial Epithelial SingleQuots Kit (Lonza, CC4175) except GA-1000 (gentamycin-amphotericin B mix), which was replaced with penicillin (100 U ml^{-1}) and streptomycin (100 μg ml^{-1}) (Sigma-Aldrich, P4333). BEAS-2B cells were seeded at a density of 2.7×10^5 cells per insert (5.8×10^4 cells cm^{-2} growth area) on 24-mm Transwell inserts with a polyester membrane, precoated with bovine collagen type 1 (0.03 mg ml^{-1}; Gibco, A1064401) and bovine serum albumin (0.01 mg ml^{-1}; Sigma-Aldrich; 9048-46-8) 4 days before the exposure experiments. Twenty-four hours after seeding, the culture medium on the apical side was removed to establish ALI conditions.

Cell exposure at the ALI

Cells were exposed at the ALI to CA or aerosol emissions using a Vitrocell Automated Exposure Station (AES) standard version (Vitrocell Systems GmbH, Germany). The cells were exposed either to total aerosol or gas-phase only, fresh, or aged aerosol emissions. The AES was operated as previously described (*47*, *88*) with similar settings used in recent studies (*20*, *48*). Briefly diluted aerosols from car exhaust were conducted through a size-selective impactor for excluding particles with size fractions > $PM_{2.5}$ and then introduced in the exposure system. Aerosol and CA (purified compressed laboratory air) were conditioned (37°C, 85% rH) and guided over the cells with a flow rate of 100 ml min^{-1}. The AES was automatically operated during the 4-hour exposure for maintaining the cells under stable temperature and RH. For gas phase-only cell exposure, glass fiber filters (Cytiva, 6723-5000) were installed directly before each inlet for removing the particles.

Shortly before exposure, 1.9-ml exposure medium, i.e., serum-free DMEM/F12 medium or complete BEGM medium supplemented with 15 mM Hepes buffer solution (Thermo Fisher Scientific, 15630-056) was added to the AES modules. Inserts with A549 and BEAS-2B cells were thereafter placed in the exposure modules containing exposure medium. The cells were exposed for 4 hours to conditioned aerosol or CA. The experiments represent three to four independent exposures. After the exposure, the cells and exposure medium were collected for direct analysis or frozen at −80°C for later analysis.

Estimation of the particle deposition in AES and in human lungs

The deposited number of particles per area is calculated using Eq. 1

$$\textit{deposited number of particles per area} = \frac{\eta \times Q \times N \times T}{A} \quad (1)$$

where Q is the aerosol flow, N is the PN concentration (particle count per volume), T is the duration of the exposure, and A is the area of the deposition plate. The size-dependent deposition efficiency of particles (η) in ALI system is calculated using the theory described in (*89*). The deposited number of particles is converted to deposited mass using the effective density of particles, as measured with the APM-SMPS setup. The mean effective density of the aged particles from the car exhaust emissions was 1.6 ± 0.7 (g cm^{-3}) over the particle size range. The method to calculate the particle deposited dose on cells in ALI system was used in previous studies (*20*, *48*).

The deposition efficiencies of the aged exhaust particles in head airways, trachea-bronchial, and alveolar regions of human lung were estimated by using simplified deposition efficiency functions based on the ICRP model results (*53*, *90*). The number size distribution of aged particles measured by SMPS and the mean effective density of particles measured by APM-SMPS were used as input data. The calculations yielded deposit fractions of PN, surface area, and mass in the previously mentioned regions of the lung.

Cytotoxicity evaluation

Cell viability was evaluated by measuring the metabolic activity of the cells after exposure. Inserts were transferred to a six-well plate, washed once with Gibco Hanks' balanced salt solution (HBSS, Thermo Fisher Scientific, 14025100), and then incubated at 37°C for 45 min with 1 ml of prewarmed exposure medium with 10 % CellTiter-Blue Cell Viability Assay (Promega, G8080) to the apical and basolateral compartments. After incubation, aliquots of the basal and apical medium were pipetted in duplicate into a 96-well plate. Absorbance at 570 nm was measured with a spectrophotometer (MULTISKAN SKY Microplate Spectrophotometer, Thermo Fisher Scientific). The results are presented as percentage of metabolic activity compared with IC from at least three independent exposures and one technical replicate, respectively.

Cell death was evaluated by measuring the release of LDH. Directly after exposure, cell media were collected from the modules and apical cell washes were performed with 1 ml of HBSS at the apical side of the inserts. LDH was measured with the Cytotoxicity Detection Kit Plus (Roche, 11644793001) according to the manufacturer's recommendation. Absorbance at 493 nm was measured with a spectrophotometer (MULTISCAN SKY Microplate Spectrophotometer). Cell culture medium was used as the blank. The results are presented as percentage of the LDH maximal release. For LDH maximal release, IC cells were washed with HBSS and basal cell medium collected 20 min before the end of the exposure, and the cells were lysed for 20 min with 2 % Triton X-100 (Sigma-Aldrich, 9036-19-5). LDH release was measured from at least three independent exposures and one to three technical replicates.

Genotoxicity evaluation

DNA single- and double-strand breaks as well as DNA oxidation were evaluated by single-cell gel electrophoresis (Comet assay). Following 4-hour exposures, both A549 and BEAS-2B cells were harvested with 0.5% Trypsin-EDTA (T4174-100ML, Sigma-Aldrich) inhibited after 5 min with FBS. The cells were then centrifuged at 200*g* for 5 min and counted with Trypan Blue (15250-061, Thermo Fisher Scientific). Cells (3×10^5 cells ml^{-1}) were resuspended in freezing medium (10 % dimethyl sulfoxide, 40 % cell culture medium, and 50 % FBS) and stored at −80°C until further analysis. The alkaline version and the enzymes modified version of Comet assay were performed as previously described (*91*). FPG FLARE Assay kit (4040_100_FM, Trevigen) and hOGG1 FLARE (4130_100_FK, Trevigen) assay kits were used in the enzyme modified Comet version. FPG and hOGG1 enzymes were diluted in FLARE buffer 1:60

and 1:100, respectively. Frozen samples were thawed and washed with cold phosphate-buffered saline (PBS). The supernatant was discarded after centrifugation at 200*g* for 10 min, and the cell density was adjusted to 2.5×10^5 cells ml^{-1} for the eight mini-gel slides preparation. Each slide thus held eight mini-gels for the different exposed samples, negative control, and two positive control conditions (1.5 mM $KBrO_3$ and 50 μM H_2O_2 for the enzymes-modified and alkaline versions, respectively). Electrophoresis was run at 0.75 V cm^{-1} and ~300 mA for 25 min, and then the slides were neutralized in 0.4 M tris solution and left to dry overnight. The slides were stained with SYBR Gold [Thermo Fisher Scientific, S11494, 1:10,000 dilution in 10 mM tris-HCl, 1 mM EDTA (pH 7.5)] and pictures taken with a Lionheart FX Automated microscope (BioTek Instruments Inc., Vermont, USA). Hundred comets per gel were scored using CometScore software (TriTek Corp., Sumerduck, VA). Percentage of DNA in the comet tail (% DNA in tail) was considered as descriptor of DNA damage. The net Fpg and hOGG1 sites were calculated by subtracting the mean values of % DNA in tail obtained in buffer without added enzymes treatments from the mean values obtained in the Fpg or hOGG1 enzyme treated slides. (Oxidative) DNA damage was analyzed from three biological replicates, and results are presented as means ± standard error of the mean (s.e.m.). DNA damage in treated samples is compared to negative controls, i.e., ICs for the alkaline comet and CA controls for the enzymes modified version.

Oxidative stress analysis

GSH/GSSG content, an indicator of oxidative stress, was quantified by LC-MS (LC-MS/MS) adapting methods previously described by Herzog *et al.* (*92*) and Sun *et al.* (*93*). The analysis was performed in positive multiple reaction monitoring (MRM) mode on an Agilent 1260 HPLC system coupled to an Agilent 6470 tandem mass spectrometer. For sample preparation, after exposure, the cells were washed twice with an ice-cold solution of 1 mM *N*-ethylmaleimide (NEM, Sigma-Aldrich, St. Louis, MO, USA) in PBS from the apical and basolateral side directly after exposure end. The wash solution was removed, and a precipitation solution consisting of ice-cold 20 mM NEM, methanol, and water was added to the apical and basolateral side, together with 20 μl of internal standard solution. After a reaction time of 5 min on ice, the inserts were scraped from both sides and the solution transferred to an Eppendorf tube. The solution was then thoroughly vortexed and centrifuged at 10,000*g* for 7 min at 4°C. The supernatant was transferred to another tube and evaporated under nitrogen at 45°C, and the residue was reconstituted in 100 μl of 0.1 % formic acid. In addition, the cells were treated with 100 μM menadione (AppliChem PanReac, Darmstadt, Germany) as positive control. For analysis of GSSG, 5 μl of the extract was injected to the HPLC system equipped with a C18 column (Penomenex Kinetex 100 mm by 2,1 mm) running a gradient elution program at 20°C column oven temperature. The mobile phase was A 0.1 % formic acid and B methanol. Mass spectrometric detection was done in positive MRM mode. For measuring GS-NEM, a 100 X dilution step was done before injecting the extract to achieve quantification in the linear calibration range of the instrument. Results are presented as the GSSG percentage of total glutathione (sum of measured GS-NEM and GSSG) from four biological replicates (one technical replicate per exposure).

MDA release, an indicator of cellular oxidative stress related to lipid peroxidation, was measured from the frozen collected sample media. Analysis was performed by LC-MS/MS in positive MRM mode on an Agilent 1260 HPLC system coupled to an Agilent 6470 triple quadrupole mass spectrometer. Sample preparation was carried out as previously described with minor changes (*94*). Briefly, after thawing the samples at room temperature, 20 μl of cell medium was added to 500 μl of 0.5 mM DNPH (Sigma-Aldrich; D199303) in 1% formic acid solution together with 20 μl of d2-MDA 33 ng ml^{-1}, acting as internal standard. For derivatization, the samples were shaken at 300 rpm and 37°C for 70 min in a Thermomixer C (Eppendorf) followed by a 30-s liquid-liquid extraction step with 600 μl of *n*-hexane. The solution was centrifuged at 10*g* for 5 min in a Heraeus Biofuge Pico Centrifuge (Thermo Fisher Scientific), and the *n*-hexane supernatant was collected. The extraction procedure was repeated once. The collected *n*-hexane supernatants were then combined and dried under a gentle stream of nitrogen in a Vapotherm Basis Mobil I (Barkey) at room temperature. The dried residue was redissolved in 50 μl of methanol:0.1 % formic acid (80:20, v/v). The extract was then injected to the HPLC system equipped with a C18 column running under isocratic condition and using a constant flow of 200 μl min^{-1} of mobile phase, followed by an MS/MS detection in MRM mode. Each sample was injected twice with 5 μl of injection volume for each measurement. A standard calibration curve with standard concentrations of MDA ranging from 0.5 to 20 ng ml^{-1} was set up for quantification. Data are presented as MDA in nanograms per milliliter. MDA release was measured from three biological replicates (one technical replicate per exposure).

Proinflammatory response

IL-8 and IL-6 release was measured in exposure media, as indicator of inflammation. Briefly, exposure media were collected directly after exposure and stored at −80°C until further analysis. IL-8 and IL-6 concentrations were measured by using the enzyme-based immunosorbent assay (R&D Systems; DY208), according to the manufacturer's instruction. Results are presented as IL-8 or IL-6 in picograms per milliliter from four independent exposures with one technical replicate each. IL-6 concentration was below the detection level in exposure media from A549 cells.

Statistical analysis

The data for the cell viability, cytotoxicity, DNA damage, MDA levels, GSSG/GSH content, and cytokine levels are expressed as the means ± s.e.m. Data were obtained from three to four independent experiments. Differences between group means were tested by one-way analysis of variance (ANOVA). Differences were considered significant at a probability level of $P < 0.05$ using Tukey's honestly significant difference hypothesis testing. Complementary two-tailed unpaired *t* test was performed between two aerosol conditions (fresh versus aged and total aerosol versus gas phase) and is specified in the respective figure. The statistical analysis and the generation of the graphs were performed with GraphPad 9 software (GraphPad Software La Jolla, CA 92037, USA). Variation of physical-chemical aerosol properties are given as means ± one SD, *t* tests were conducted using Statistics Toolbox of MATLAB (The MathWorks Inc., version 2024; MA, USA.

Supplementary Materials

This PDF file includes:

Figs. S1 to S7

Tables S1 to S5

REFERENCES AND NOTES

1. M. Stafoggia, B. Oftedal, J. Chen, S. Rodopoulou, M. Renzi, R. W. Atkinson, M. Bauwelinck, J. O. Klompmaker, A. Mehta, D. Vienneau, Z. J. Andersen, T. Bellander, J. Brandt, G. Cesaroni, K. de Hoogh, D. Fecht, J. Gulliver, O. Hertel, B. Hoffmann, U. A. Hvidtfeldt, K. H. Jöckel, J. T. Jørgensen, K. Katsouyanni, M. Ketzel, D. T. Kristoffersen, A. Lager, K. Leander, S. Liu, P. L. S. Ljungman, G. Nagel, G. Pershagen, A. Peters, O. Raaschou-Nielsen, D. Rizzuto, S. Schramm, P. E. Schwarze, G. Severi, T. Sigsgaard, M. Strak, Y. T. van der Schouw, M. Verschuren, G. Weinmayr, K. Wolf, E. Zitt, E. Samoli, F. Forastiere, B. Brunekreef, G. Hoek, N. A. H. Janssen, Long-term exposure to low ambient air pollution concentrations and mortality among 28 million people: Results from seven large European cohorts within the ELAPSE project. *Lancet Planet Health* **6**, e9–e18 (2022).
2. A. J. Cohen, M. Brauer, R. Burnett, H. R. Anderson, J. Frostad, K. Estep, K. Balakrishnan, B. Brunekreef, L. Dandona, R. Dandona, V. Feigin, G. Freedman, B. Hubbell, A. Jobling, H. Kan, L. Knibbs, Y. Liu, R. Martin, L. Morawska, C. A. Pope, H. Shin, K. Straif, G. Shaddick, M. Thomas, R. van Dingenen, A. van Donkelaar, T. Vos, C. J. L. Murray, M. H. Forouzanfar, Estimates and 25-year trends of the global burden of disease attributable to ambient air pollution: An analysis of data from the Global Burden of Diseases Study 2015. *Lancet* **389**, 1907–1918 (2017).
3. P. Orellano, J. Reynoso, N. Quaranta, A. Bardach, A. Ciapponi, Short-term exposure to particulate matter (PM_{10} and $PM_{2.5}$), nitrogen dioxide (NO_2), and ozone (O_3) and all-cause and cause-specific mortality: Systematic review and meta-analysis. *Environ. Int.* **142**, 105876 (2020).
4. S. Weichenthal, L. Pinault, T. Christidis, R. T. Burnett, J. R. Brook, Y. Chu, D. L. Crouse, A. C. Erickson, P. Hystad, C. Li, R. V. Martin, J. Meng, A. J. Pappin, M. Tjepkema, A. van Donkelaar, C. L. Weagle, M. Brauer, How low can you go? Air pollution affects mortality at very low levels. *Sci. Adv.* **8**, 3381 (2022).
5. X. Zhu, Q. Zhang, X. Du, Y. Jiang, Y. Niu, Y. Wei, Y. Zhang, S. N. Chillrud, D. Liang, H. Li, R. Chen, H. Kan, J. Cai, Respiratory effects of traffic-related air pollution: A randomized, crossover analysis of lung function, airway metabolome, and biomarkers of airway injury. *Environ. Health Perspect.* **131**, 57002 (2023).
6. L. D. Claxton, The history, genotoxicity, and carcinogenicity of carbon-based fuels and their emissions. Part 3: Diesel and gasoline. *Mutat. Res.* **763**, 30–85 (2015).
7. S. Edwards, G. Zhao, J. Tran, K. T. Patten, A. Valenzuela, C. Wallis, K. J. Bein, A. S. Wexler, P. J. Lein, X. Rao, Pathological cardiopulmonary evaluation of rats chronically exposed to traffic-related air pollution. *Environ. Health Perspect.* **128**, 127003 (2020).
8. E. Long, C. Carlsten, Controlled human exposure to diesel exhaust: Results illuminate health effects of traffic-related air pollution and inform future directions. *Part Fibre Toxicol.* **19**, 11 (2022).
9. A. A. May, N. T. Nguyen, A. A. Presto, T. D. Gordon, E. M. Lipsky, M. Karve, A. Gutierrez, W. H. Robertson, M. Zhang, C. Brandow, O. Chang, S. Chen, P. Cicero-Fernandez, L. Dinkins, M. Fuentes, S. M. Huang, R. Ling, J. Long, C. Maddox, J. Massetti, E. McCauley, A. Miguel, K. Na, R. Ong, Y. Pang, P. Rieger, T. Sax, T. Truong, T. Vo, S. Chattopadhyay, H. Maldonado, M. M. Maricq, A. L. Robinson, Gas- and particle-phase primary emissions from in-use, on-road gasoline and diesel vehicles. *Atmos. Environ.* **88**, 247–260 (2014).
10. G. Saliba, R. Saleh, Y. Zhao, A. A. Presto, A. T. Lambe, B. Frodin, S. Sardar, H. Maldonado, C. Maddox, A. A. May, G. T. Drozd, A. H. Goldstein, L. M. Russell, F. Hagen, A. L. Robinson, Comparison of gasoline direct-injection (GDI) and port fuel injection (PFI) vehicle emissions: Emission certification standards, cold-start, secondary organic aerosol formation potential, and potential climate impacts. *Environ. Sci. Technol.* **51**, 6542–6552 (2017).
11. O. I. Awad, X. Ma, M. Kamil, O. M. Ali, Z. Zhang, S. Shuai, Particulate emissions from gasoline direct injection engines: A review of how current emission regulations are being met by automobile manufacturers. *Sci. Total Environ.* **718**, 137302 (2020).
12. A. Joshi, T. V. Johnson, Gasoline particulate filters—A review. *Emiss. Contr. Sci. Tech.* **4**, 219–239 (2018).
13. J. Usemann, M. Roth, C. Bisig, P. Comte, J. Czerwinski, A. C. R. Mayer, P. Latzin, L. Müller, Gasoline particle filter reduces oxidative DNA damage in bronchial epithelial cells after whole gasoline exhaust exposure in vitro. *Sci. Rep.* **8**, 2297 (2018).
14. C. Bisig, P. Comte, M. Güdel, J. Czerwinski, A. Mayer, L. Müller, A. Petri-Fink, B. Rothen-Rutishauser, Assessment of lung cell toxicity of various gasoline engine exhausts using a versatile in vitro exposure system. *Environ. Pollut.* **235**, 263–271 (2018).
15. M. Hallquist, J. C. Wenger, U. Baltensperger, Y. Rudich, D. Simpson, M. Claeys, J. Dommen, N. M. Donahue, C. George, A. H. Goldstein, J. F. Hamilton, H. Herrmann, T. Hoffmann, Y. Iinuma, M. Jang, M. E. Jenkin, J. L. Jimenez, A. Kiendler-Scharr, W. Maenhaut, G. McFiggans, T. F. Mentel, A. Monod, A. S. H. Prévôt, J. H. Seinfeld, J. D. Surratt, R. Szmigielski, J. Wildt, The formation, properties and impact of secondary organic aerosol: Current and emerging issues. *Atmos. Chem. Phys.* **9**, 5155–5236 (2009).
16. J. H. Kroll, N. M. Donahue, J. L. Jimenez, S. H. Kessler, M. R. Canagaratna, K. R. Wilson, K. E. Altieri, L. R. Mazzoleni, A. S. Wozniak, H. Bluhm, E. R. Mysak, J. D. Smith, C. E. Kolb, D. R. Worsnop, Carbon oxidation state as a metric for describing the chemistry of atmospheric organic aerosol. *Nat. Chem.* **3**, 133–139 (2011).
17. H. O. T. Pye, C. K. Ward-Caviness, B. N. Murphy, K. W. Appel, K. M. Seltzer, Secondary organic aerosol association with cardiorespiratory disease mortality in the United States. *Nat. Commun.* **12**, 7215 (2021).
18. K. Von Stackelberg, J. Buonocore, P. V. Bhave, J. A. Schwartz, Public health impacts of secondary particulate formation from aromatic hydrocarbons in gasoline. *Environ. Health* **12**, 19 (2013).
19. D. R. Gentner, S. H. Jathar, T. D. Gordon, R. Bahreini, D. A. Day, I. El Haddad, P. L. Hayes, S. M. Pieber, S. M. Platt, J. de Gouw, A. H. Goldstein, R. A. Harley, J. L. Jimenez, S. H. Pre, A. L. Robinson, Review of urban secondary organic aerosol formation from gasoline and diesel motor vehicle emissions. *Environ. Sci. Technol.* **51**, 1074–7093 (2017).
20. S. Offer, E. Hartner, S. Di Bucchianico, C. Bisig, S. Bauer, J. Pantzke, E. J. Zimmermann, X. Cao, S. Binder, E. Kuhn, A. Huber, S. Jeong, U. Käfer, P. Martens, A. Mesceriakovas, J. Bendl, R. Brejcha, A. Buchholz, D. Gat, T. Hohaus, N. Rastak, G. Jakobi, M. Kalberer, T. Kanashova, Y. Hu, C. Ogris, A. Marsico, F. Theis, M. Pardo, T. Gröger, S. Oeder, J. Orasche, A. Paul, T. Ziehm, Z.-H. Zhang, T. Adam, O. Sippula, M. Sklorz, J. Schnelle-Kreis, H. Czech, A. Kiendler-Scharr, Y. Rudich, R. Zimmermann, Effect of atmospheric aging on soot particle toxicity in lung cell models at the air–liquid interface: Differential toxicological impacts of biogenic and anthropogenic secondary organic aerosols (SOAs). *Environ. Health Perspect.* **130**, 027003 (2022).
21. M. Pardo, S. Offer, E. Hartner, S. Di Bucchianico, C. Bisig, S. Bauer, J. Pantzke, E. J. Zimmermann, X. Cao, S. Binder, E. Kuhn, A. Huber, S. Jeong, U. Käfer, E. Schneider, A. Mesceriakovas, J. Bendl, R. Brejcha, A. Buchholz, D. Gat, T. Hohaus, N. Rastak, E. Karg, G. Jakobi, M. Kalberer, T. Kanashova, Y. Hu, C. Ogris, A. Marsico, F. Theis, T. Shalit, T. Gröger, C. P. Rüger, S. Oeder, J. Orasche, A. Paul, T. Ziehm, Z. H. Zhang, T. Adam, O. Sippula, M. Sklorz, J. Schnelle-Kreis, H. Czech, A. Kiendler-Scharr, R. Zimmermann, Y. Rudich, Exposure to naphthalene and β-pinene-derived secondary organic aerosol induced divergent changes in transcript levels of BEAS-2B cells. *Environ. Int.* **166**, 107366 (2022).
22. Z. H. Zhang, E. Hartner, B. Utinger, B. Gfeller, A. Paul, M. Sklorz, H. Czech, B. X. Yang, X. Y. Su, G. Jakobi, J. Orasche, J. Schnelle-Kreis, S. Jeong, T. Gröger, M. Pardo, T. Hohaus, T. Adam, A. Kiendler-Scharr, Y. Rudich, R. Zimmermann, M. Kalberer, Are reactive oxygen species (ROS) a suitable metric to predict toxicity of carbonaceous aerosol particles? *Atmos. Chem. Phys.* **22**, 1793–1809 (2022).
23. L. Pirjola, P. Karjalainen, J. Heikkilä, S. Saari, T. Tzamkiozis, L. Ntziachristos, K. Kulmala, J. Keskinen, T. Rönkkö, Effects of fresh lubricant oils on particle emissions emitted by a modern gasoline direct injection passenger car. *Environ. Sci. Technol.* **49**, 3644–3652 (2015).
24. T. D. Gordon, D. S. Tkacik, A. A. Presto, M. Zhang, S. H. Jathar, N. T. Nguyen, J. Massetti, T. Truong, P. Cicero-Fernandez, C. Maddox, P. Rieger, S. Chattopadhyay, H. Maldonado, M. M. Maricq, A. L. Robinson, Primary gas-and particle-phase emissions and secondary organic aerosol production from gasoline and diesel off-road engines. *Atmos. Chem. Phys.* **14**, 4643–4659 (2014).
25. L. Künzi, M. Krapf, N. Daher, J. Dommen, N. Jeannet, S. Schneider, S. Platt, J. G. Slowik, N. Baumlin, M. Salathe, A. S. H. Prévôt, M. Kalberer, C. Strähl, L. Dümbgen, C. Sioutas, U. Baltensperger, M. Geiser, Toxicity of aged gasoline exhaust particles to normal and diseased airway epithelia. *Sci. Rep.* **5**, 11801 (2015).
26. Y. S. Lau, H. Y. Poon, B. Organ, H. C. Chuang, M. N. Chan, H. Guo, S. S. H. Ho, K. F. Ho, Toxicological effects of fresh and aged gasoline exhaust particles in Hong Kong. *J. Hazard. Mater.* **441**, 129846 (2023).
27. A. Järvinen, H. Timonen, P. Karjalainen, M. Bloss, P. Simonen, S. Saarikoski, H. Kuuluvainen, J. Kalliokoski, M. Dal Maso, J. V. Niemi, J. Keskinen, T. Rönkkö, Particle emissions of Euro VI, EEV and retrofitted EEV city buses in real traffic. *Environ. Pollut.* **250**, 708–716 (2019).
28. S. M. Pieber, N. K. Kumar, F. Klein, P. Comte, D. Bhattu, J. Dommen, E. A. Bruns, D. Kiluic, I. El Haddad, A. Keller, J. Czerwinski, N. Heeb, U. Baltensperger, J. G. Slowik, A. S. H. Prévôt, Gas-phase composition and secondary organic aerosol formation from standard and particle filter-retrofitted gasoline direct injection vehicles investigated in a batch and flow reactor. *Atmos. Chem. Phys.* **18**, 9929–9954 (2018).
29. A. H. Hartikainen, M. Ihalainen, P. Yli-Pirilä, L. Hao, M. Kortelainen, S. M. Pieber, O. Sippula, Photochemical transformation and secondary aerosol formation potential of Euro6 gasoline and diesel passenger car exhaust emissions. *J. Aerosol Sci.* **171**, 106159 (2023).
30. M. Kraft, T. Eikmann, A. Kappos, N. Künzli, R. Rapp, K. Schneider, H. Seitz, J. U. Voss, H. E. Wichmann, The German view: Effects of nitrogen dioxide on human health – derivation of health-related short-term and long-term values. *Int. J. Hyg. Environ. Health* **208**, 305–318 (2005).
31. J. E. Goodman, R. L. Prueitt, S. N. Sax, D. M. Pizzurro, H. N. Lynch, K. Zu, F. J. Venditti, Ozone exposure and systemic biomarkers: Evaluation of evidence for adverse cardiovascular health impacts. *Crit. Rev. Toxicol.* **45**, 412–452 (2015).
32. T. Karl, C. Lamprecht, M. Graus, A. Cede, M. Tiefengraber, J. V. G. de Arellano, D. Gurarie, D. Lenschow, High urban NO_x triggers a substantial chemical downward flux of ozone. *Sci. Adv.* **9**, eadd2365 (2023).
33. W. P. Carter, Development of ozone reactivity scales for volatile organic compounds. *Air Waste* **44**, 881–899 (1994).

34. WHO, *WHO Global Air Quality Guidelines. Particulate Matter (PM2.5 and PM 10), Ozone, Nitrogen Dioxide, Sulfur Dioxide and Carbon Monoxide.* (World Health Organization, Geneva, 2021).
35. M. Ihalainen, P. Tiitta, H. Czech, P. Yli-Pirilä, A. Hartikainen, M. Kortelainen, J. Tissari, B. Stengel, M. Sklorz, H. Suhonen, H. Lamberg, A. Leskinen, A. Kiendler-Scharr, H. Harndorf, R. Zimmermann, J. Jokiniemi, O. Sippula, A novel high-volume PHOTOCHEMICAL EMISSION AGING FLOW TUBE REActor (PEAR). *Aerosol Sci. Tech.* **53**, 276–294 (2019).
36. P. S. K. Liu, R. Deng, K. A. Smith, L. R. Williams, J. T. Jayne, M. R. Canagaratna, K. Moore, T. B. Onasch, D. R. Worsnop, T. Deshler, Transmission efficiency of an aerodynamic focusing lens system: Comparison of model calculations and laboratory measurements for the aerodyne aerosol mass spectrometer. *Aerosol Sci. Tech.* **41**, 721–733 (2007).
37. F. Liu, T. Xu, N. L. Ng, H. Lu, Linking cell health and reactive oxygen species from secondary organic aerosols exposure. *Environ. Sci. Technol.* **57**, 1039–1048 (2023).
38. H. Jiang, M. Jang, T. Sabo-Attwood, S. E. Robinson, Oxidative potential of secondary organic aerosols produced from photooxidation of different hydrocarbons using outdoor chamber under ambient sunlight. *Atmos. Environ.* **131**, 382–389 (2016).
39. N. L. Ng, M. R. Canagaratna, J. L. Jimenez, P. S. Chhabra, J. H. Seinfeld, D. R. Worsnop, Changes in organic aerosol composition with aging inferred from aerosol mass spectra. *Atmos. Chem. Phys.* **11**, 6465–6474 (2011).
40. B. Alexander, T. Sherwen, C. D. Holmes, J. A. Fisher, Q. Chen, M. J. Evans, P. Kasibhatla, Global inorganic nitrate production mechanisms: Comparison of a global model with nitrate isotope observations. *Atmos. Chem. Phys.* **20**, 3859–3877 (2020).
41. H. Czech, B. Stengel, T. Adam, M. Sklorz, T. Streibel, R. Zimmermann, A chemometric investigation of aromatic emission profiles from a marine engine in comparison with residential wood combustion and road traffic: Implications for source apportionment inside and outside sulphur emission control areas. *Atmos. Environ.* **167**, 212–222 (2017).
42. R. Atkinson, J. Arey, Atmospheric degradation of volatile organic compounds. *Chem. Rev.* **103**, 4605–4638 (2003).
43. G. Lacroix, W. Koch, D. Ritter, A. C. Gutleb, S. T. Larsen, T. Loret, F. Zanetti, S. Constant, S. Chortarea, B. Rothen-Rutishauser, P. S. Hiemstra, E. Frejafon, P. Hubert, L. Gribaldo, P. Kearns, J. M. Aublant, S. Diabaté, C. Weiss, A. De Groot, I. Kooter, Air–liquid interface in vitro models for respiratory toxicology research: Consensus workshop and recommendations. *Appl. In Vitro Toxicol.* **4**, 91–106 (2018).
44. H. R. Paur, F. R. Cassee, J. Teeguarden, H. Fissan, S. Diabate, M. Aufderheide, W. G. Kreyling, O. Hänninen, G. Kasper, M. Riediker, B. Rothen-Rutishauser, O. Schmid, In-vitro cell exposure studies for the assessment of nanoparticle toxicity in the lung-A dialog between aerosol science and biology. *J. Aerosol Sci.* **42**, 668–692 (2011).
45. C. A. Weitekamp, T. Stevens, M. J. Stewart, P. Bhave, M. I. Gilmour, Health effects from freshly emitted versus oxidatively or photochemically aged air pollutants. *Sci Total Environ.* **704**, 135772 (2020).
46. D. Walczyk, F. B. Bombelli, M. P. Monopoli, I. Lynch, K. A. Dawson, What the cell "sees" in bionanoscience. *J. Am. Chem. Soc.* **132**, 5761–5768 (2010).
47. S. Oeder, T. Kanashova, O. Sippula, S. C. Sapcariu, T. Streibel, J. M. Arteaga-Salas, J. Passig, M. Dilger, H.-R. Paur, C. Schlager, S. Mülhopt, S. Diabaté, C. Weiss, B. Stengel, R. Rabe, H. Harndorf, T. Torvela, J. K. Jokiniemi, M.-R. Hirvonen, C. Schmidt-Weber, C. Traidl-Hoffmann, K. A. BéruBé, A. J. Wlodarczyk, Z. Prytherch, B. Michalke, T. Krebs, A. S. H. Prévôt, M. Kelbg, J. Tiggesbäumker, E. Karg, G. Jakobi, S. Scholtes, J. Schnelle-Kreis, J. Lintelmann, G. Matuschek, M. Sklorz, S. Klingbeil, J. Orasche, P. Richthammer, L. Müller, M. Elsasser, A. Reda, T. Gröger, B. Weggler, T. Schwemer, H. Czech, C. P. Rüger, G. Abbaszade, C. Radischat, K. Hiller, J. T. M. Buters, G. Dittmar, R. Zimmermann, Particulate matter from both heavy fuel oil and diesel fuel shipping emissions show strong biological effects on human lung cells at realistic and comparable in vitro exposure conditions. *PLOS ONE* **10**, e0126536 (2015).
48. E. J. Zimmermann, J. Candeias, N. Gawlitta, C. Bisig, S. Binder, J. Pantzke, S. Offer, N. Rastak, S. Bauer, A. Huber, E. Kuhn, J. Buters, T. Groeger, M. N. Delaval, S. Oeder, S. Di Bucchianico, R. Zimmermann, Biological impact of sequential exposures to allergens and ultrafine particle-rich combustion aerosol on human bronchial epithelial BEAS-2B cells at the air liquid interface. *J. Appl. Toxicol.* **43**, 1225–1241 (2023).
49. C. Méausoone, Y. Landkocz, F. Cazier, M. Seigneur, D. Courcot, S. Billet, Toxicological responses of BEAS-2B cells to repeated exposures to benzene, toluene, m-xylene, and mesitylene using air–liquid interface method. *J. Appl. Toxicol.* **41**, 1262–1274 (2021).
50. M. Mascelloni, J. M. Delgado-Saborit, N. J. Hodges, R. M. Harrison, Study of gaseous benzene effects upon A549 lung epithelial cells using a novel exposure system. *Toxicol. Lett.* **237**, 38–45 (2015).
51. S. Binder, N. Rastak, E. Karg, A. Huber, E. Kuhn, G. C. Dragan, C. Monsé, D. Breuer, S. Di Bucchianico, M. N. Delaval, S. Oeder, M. Sklorz, R. Zimmermann, Construction of an in vitro air-liquid interface exposure system to assess the toxicological impact of gas and particle phase of semi-volatile organic compounds. *Toxics* **10**, 730 (2022).
52. H. Hakkarainen, P. Aakko-Saksa, M. Sainio, T. Ihantola, T. J. Rönkkö, P. Koponen, T. Rönkkö, P. I. Jalava, Toxicological evaluation of exhaust emissions from light-duty vehicles using different fuel alternatives in sub-freezing conditions. *Part. Fibre Toxicol.* **17**, 17 (2020).
53. ICRP, *Human Respiratory Tract Model for Radiological Protection* (ICRP Publication 66., 1994), vol. 24; https://icrp.org/publication.asp?id=ICRP%20Publication%2066.
54. P. S. Gilmour, I. Rahman, K. Donaldson, W. MacNee, Histone acetylation regulates epithelial IL-8 release mediated by oxidative stress from environmental particles. *Am. J. Physiol. Lung Cell. Mol. Physiol.* **284**, 533–540 (2003).
55. B. S. Qazi, K. Tang, A. Qazi, Recent advances in underlying pathologies provide insight into interleukin-8 expression-mediated inflammation and angiogenesis. *Int. J. Inflam.* **2011**, 908468 (2011).
56. M. Pardo, H. Czech, S. Offer, M. Sklorz, S. Di Bucchianico, E. Hartner, J. Pantzke, E. Kuhn, A. Paul, T. Ziehm, Z. H. Zhang, G. Jakobi, S. Bauer, A. Huber, E. J. Zimmermann, N. Rastak, S. Binder, R. Brejcha, E. Schneider, J. Orasche, C. P. Rüger, T. Gröger, S. Oeder, J. Schnelle-Kreis, T. Hohaus, M. Kalberer, O. Sippula, A. Kiendler-Scharr, R. Zimmermann, Y. Rudich, Atmospheric aging increases the cytotoxicity of bare soot particles in BEAS-2B lung cells. *Aerosol Sci. Tech.* **57**, 367–383 (2023).
57. L. P. da Silva Sergio, A. L. Mencalha, A. de Souza da Fonseca, F. de Paoli, DNA repair and genomic stability in lungs affected by acute injury. *Biomed. Pharmacother.* **119**, 109412 (2019).
58. P. Rossner, T. Cervena, M. Vojtisek-Lom, K. Vrbova, A. Ambroz, Z. Novakova, F. Elzeinova, H. Margaryan, V. Beranek, M. Pechout, D. Macoun, J. Klema, A. Rossnerova, M. Ciganek, J. Topinka, The biological effects of complete gasoline engine emissions exposure in a 3D human airway model (Mucilairtm) and in human bronchial epithelial cells (BEAS-2B). *Int. J. Mol. Sci.* **20**, 5710 (2019).
59. T. Cervena, M. Vojtisek-Lom, K. Vrbova, A. Ambroz, Z. Novakova, F. Elzeinova, M. Sima, V. Beranek, M. Pechout, D. Macoun, J. Klema, A. Rossnerova, M. Ciganek, J. Topinka, P. Rossner, Ordinary gasoline emissions induce a toxic response in bronchial cells grown at air-liquid interface. *Int. J. Mol. Sci.* **22**, 79 (2020).
60. B. Novotná, J. Sikorová, A. Milcová, M. Pechout, L. Dittrich, M. Vojtíšek-Lom, P. Rossner, T. Brzicová, J. Topinka, The genotoxicity of organic extracts from particulate truck emissions produced at various engine operating modes using diesel or biodiesel (B100) fuel: A pilot study. *Mutat. Res. Genet. Toxicol. Environ. Mutagen.* **845**, 403034 (2019).
61. E. G. Tzortzaki, K. Dimakou, E. Neofytou, K. Tsikritsaki, K. Samara, M. Avgousti, V. Amargianitakis, A. Gousiou, S. Menikou, N. M. Siafakas, Oxidative DNA damage and somatic mutations: A link to the molecular pathogenesis of chronic inflammatory airway diseases. *Chest* **141**, 1243–1250 (2012).
62. C. F. dos Santos, M. G. Braz, N. M. de Arruda, L. Caram, D. L. Nogueira, S. E. Tanni, I. de Godoy, R. Ferrari, DNA damage and antioxidant capacity in COPD patients with and without lung cancer. *PLOS ONE* **17**, e0275873 (2022).
63. S. Upadhyay, L. Palmberg, Air-liquid interface: Relevant in vitro models for investigating air pollutant-induced pulmonary toxicity. *Toxicol. Sci.* **164**, 21–30 (2018).
64. T. S. Adams, A. Marlier, N. Kaminski, Lung cell atlases in health and disease. *Annu. Rev. Physiol.* **85**, 47–69 (2023).
65. M. Aghapour, N. D. Ubags, D. Bruder, P. S. Hiemstra, V. Sidhaye, F. Rezaee, I. H. Heijink, Role of air pollutants in airway epithelial barrier dysfunction in asthma and COPD. *Eur. Respir. Rev.* **31**, 210112 (2022).
66. H. Hakkarainen, A. Järvinen, T. Lepistö, L. Salo, N. Kuittinen, E. Laakkonen, M. Yang, M. V. Martikainen, S. Saarikoski, M. Aurela, L. Barreira, K. Teinilä, M. Ihalainen, P. Aakko-Saksa, H. Timonen, T. Rönkkö, P. Jalava, Toxicity of exhaust emissions from high aromatic and non-aromatic diesel fuels using in vitro ALI exposure system. *Sci. Total Environ.* **890**, 164215 (2023).
67. N. Burden, M. J. D. Clift, G. J. S. Jenkins, B. Labram, F. Sewell, Opportunities and challenges for integrating new in vitro methodologies in hazard testing and risk assessment. *Small* **17**, 2006298 (2021).
68. R. Suarez-Bertoa, V. Valverde, M. Clairotte, J. Pavlovic, B. Giechaskiel, V. Franco, Z. Kregar, C. Astorga, On-road emissions of passenger cars beyond the boundary conditions of the real-driving emissions test. *Environ. Res.* **176**, 108572 (2019).
69. Z. Peng, J. L. Jimenez, Radical chemistry in oxidation flow reactors for atmospheric chemistry research. *Chem. Soc. Rev.* **49**, 2570–2616 (2020).
70. Z. Peng, J. L. Jimenez, Modeling of the chemistry in oxidation flow reactors with high initial NO. *Atmos. Chem. Phys.* **17**, 11991–12010 (2017).
71. Z. Peng, J. Lee-Taylor, J. J. Orlando, G. S. Tyndall, J. L. Jimenez, Organic peroxy radical chemistry in oxidation flow reactors and environmental chambers and their atmospheric relevance. *Atmos. Chem. Phys.* **19**, 813–834 (2019).
72. P. Barmet, J. Dommen, P. F. DeCarlo, T. Tritscher, A. P. Praplan, S. M. Platt, A. S. H. Prévôt, N. M. Donahue, U. Baltensperger, OH clock determination by proton transfer reaction mass spectrometry at an environmental chamber. *Atmos. Meas. Tech.* **5**, 647–656 (2012).
73. R. Li, B. B. Palm, A. M. Ortega, J. Hlywiak, W. Hu, Z. Peng, D. A. Day, C. Knote, W. H. Brune, J. A. De Gouw, J. L. Jimenez, Modeling the radical chemistry in an oxidation flow reactor: Radical formation and recycling, sensitivities, and the OH exposure estimation equation. *J. Phys. Chem. A* **119**, 4418–4432 (2015).
74. Z. Peng, D. A. Day, A. M. Ortega, B. B. Palm, W. Hu, H. Stark, R. Li, K. Tsigaridis, W. H. Brune, J. L. Jimenez, Non-OH chemistry in oxidation flow reactors for the study of atmospheric chemistry systematically examined by modeling. *Atmos. Chem. Phys.* **16**, 4283–4305 (2016).

75. E. Schneider, H. Czech, A. Hartikainen, H. J. Hansen, N. Gawlitta, M. Ihalainen, P. Yli-Pirilä, M. Somero, M. Kortelainen, J. Louhisalmi, J. Orasche, Z. Fang, Y. Rudich, O. Sippula, C. P. Rüger, R. Zimmermann, Molecular composition of fresh and aged aerosols from residential wood combustion and gasoline car with modern emission mitigation technology. *Environ. Sci. Process Impacts* **26**, 1295–1309 (2024).
76. A. Paul, Z. Fang, P. Martens, A. Mukherjee, G. Jakobi, M. Ihalainen, M. Kortelainen, M. Somero, P. Yli-Pirilä, T. Hohaus, H. Czech, M. Kalberer, O. Sippula, Y. Rudich, R. Zimmermann, A. Kiendler-Scharr, Formation of secondary aerosol from emissions of a Euro 6d-compliant gasoline vehicle with a particle filter. *Environ. Sci. Atmos.* **4**, 802–812 (2024).
77. H. Czech, P. Yli-Pirilä, P. Tiitta, M. Ihalainen, A. Hartikainen, E. Schneider, P. Martens, A. Paul, T. Hohaus, C. P. Rüger, J. Jokiniemi, R. Zimmermann, O. Sippula, The effect of aging conditions at equal OH exposure in an oxidation flow reactor on the composition of toluene-derived secondary organic aerosols. *Environ. Sci. Atmos.* **4**, 718–731 (2024).
78. M. R. Canagaratna, J. L. Jimenez, J. H. Kroll, Q. Chen, S. H. Kessler, P. Massoli, L. Hildebrandt Ruiz, E. Fortner, L. R. Williams, K. R. Wilson, J. D. Surratt, N. M. Donahue, J. T. Jayne, D. R. Worsnop, Elemental ratio measurements of organic compounds using aerosol mass spectrometry: Characterization, improved calibration, and implications. *Atmos. Chem. Phys.* **15**, 253–272 (2015).
79. F. P. H. Wragg, S. J. Fuller, R. Freshwater, D. C. Green, F. J. Kelly, M. Kalberer, An automated online instrument to quantify aerosol-bound reactive oxygen species (ROS) for ambient measurement and health-relevant aerosol studies. *Atmos. Meas. Tech.* **9**, 4891–4900 (2016).
80. B. Utinger, S. J. Campbell, N. Bukowiecki, A. Barth, B. Gfeller, R. Freshwater, H.-R. Rüegg, M. Kalberer, An automated online field instrument to quantify the oxidative potential of aerosol particles via ascorbic acid oxidation. *Atmos. Meas. Tech.* **16**, 2641–2654 (2023).
81. S. J. Campbell, B. Utinger, D. M. Lienhard, S. E. Paulson, J. Shen, P. T. Griffiths, A. C. Stell, M. Kalberer, Development of a physiologically relevant online chemical assay to quantify aerosol oxidative potential. *Anal. Chem.* **91**, 13088–13095 (2019).
82. J. Lyyränen, U. Backman, U. Tapper, A. Auvinen, J. Jokiniemi, A size selective nanoparticle collection device based on diffusion and thermophoresis. *J. Phys. Conf. Ser.* **170**, 012011 (2009).
83. J. Leskinen, M. Ihalainen, T. Torvela, M. Kortelainen, H. Lamberg, P. Tiitta, G. Jakobi, J. Grigonyte, J. Joutsensaari, O. Sippula, J. Tissari, A. Virtanen, R. Zimmermann, J. Jokiniemi, Effective density and morphology of particles emitted from small-scale combustion of various wood fuels. *Environ. Sci. Technol.* **48**, 13298–13306 (2014).
84. M. Graus, M. Müller, A. Hansel, High resolution PTR-TOF: Quantification and formula confirmation of VOC in real time. *J. Am. Soc. Mass Spectrom.* **21**, 1037–1044 (2010).
85. L. Cappellin, T. Karl, M. Probst, O. Ismailova, P. M. Winkler, C. Soukoulis, E. Aprea, T. D. Märk, F. Gasperi, F. Biasioli, On quantitative determination of volatile organic compound concentrations using proton transfer reaction time-of-flight mass spectrometry. *Environ. Sci. Technol.* **46**, 2283–2290 (2012).
86. C. Gehm, T. Streibel, J. Passig, R. Zimmermann, Determination of relative ionization cross sections for resonance enhanced multiphoton ionization of polycyclic aromatic hydrocarbons. *Appl. Sci.* **8**, 1617 (2018).
87. H. Czech, O. Sippula, M. Kortelainen, J. Tissari, C. Radischat, J. Passig, T. Streibel, J. Jokiniemi, R. Zimmermann, On-line analysis of organic emissions from residential wood combustion with single-photon ionisation time-of-flight mass spectrometry (SPI-TOFMS). *Fuel* **177**, 334–342 (2016).
88. S. Mülhopt, M. Dilger, S. Diabaté, C. Schlager, T. Krebs, R. Zimmermann, J. Buters, S. Oeder, T. Wäscher, C. Weiss, H. R. Paur, Toxicity testing of combustion aerosols at the air–liquid interface with a self-contained and easy-to-use exposure system. *J. Aerosol Sci.* **96**, 38–55 (2016).
89. F. Lucci, N. D. Castro, A. A. Rostami, M. J. Oldham, J. Hoeng, Y. B. Pithawalla, A. K. Kuczaj, Characterization and modeling of aerosol deposition in Vitrocell® exposure systems - Exposure well chamber deposition efficiency. *J. Aerosol Sci.* **123**, 141–160 (2018).
90. T. Lepistö, H. Kuuluvainen, P. Juuti, A. Järvinen, A. Arffman, T. Rönkkö, Measurement of the human respiratory tract deposited surface area of particles with an electrical low pressure impactor. *Aerosol Sci. Tech.* **54**, 958–971 (2020).
91. S. Di Bucchianico, F. Cappellini, F. Le Bihanic, Y. Zhang, K. Dreij, H. L. Karlsson, Genotoxicity of TiO_2 nanoparticles assessed by mini-gel comet assay and micronucleus scoring with flow cytometry. *Mutagenesis* **32**, 127–137 (2017).
92. K. Herzog, L. Ijlst, A. G. van Cruchten, C. W. T. van Roermund, W. Kulik, R. J. A. Wanders, H. R. Waterham, An UPLC-MS/MS assay to measure glutathione as marker for oxidative stress in cultured cells. *Metabolites* **9**, 45 (2019).
93. X. Sun, R. S. Berger, P. Heinrich, I. Marchiq, J. Pouyssegur, K. Renner, P. J. Oefner, K. Dettmer, Optimized protocol for the in situ derivatization of glutathione with *N*-ethylmaleimide in cultured cells and the simultaneous determination of glutathione/glutathione disulfide ratio by HPLC-UV-QTOF-MS. *Metabolites* **10**, 292 (2020).
94. X. Wu, J. Lintelmann, S. Klingbeil, J. Li, H. Wang, E. Kuhn, S. Ritter, R. Zimmermann, Determination of air pollution-related biomarkers of exposure in urine of travellers between Germany and China using liquid chromatographic and liquid chromatographic-mass spectrometric methods: A pilot study. *Biomarkers* **22**, 525–536 (2017).

Acknowledgments

Funding: This work was supported by the following: Helmholtz International Laboratory aeroHEALTH (InterLabs-0005) (R.Z., Y.R., and A.K.-S.); Helmholtz Virtual Institute of Complex Molecular Systems in Environmental Health - Aerosols and Health (HICE) (R.Z.); H2020 EU project ULtrafine particles from TRansportation - Health Assessment of Source (ULTRHAS, grant no. 955390) (R.Z. and S.D.B.); Research Council of Finland project BBrCAC (grant no. 341597) (O.S.); EDUFI Fellowship Grant from the Finnish National Agency for Education (TM-21-11567) (A.Mu.); LUMETO Doctoral Fellowship provided by the University of Eastern Finland (A.Mu.); and Research Council of Finland competitive funding to strengthen university research profiles (PROFI) for the University of Eastern Finland (M.I.). This research was supported by EU Horizon 2020 project ULTRHAS – ULtrafine particles from TRansportation – Health Assessment of Sources, grant agreement no. 955390. Views and opinions expressed are, however, those of the authors only and do not necessarily reflect those of the European Union. Neither the European Union nor the granting authority can be held responsible for them. **Author contributions:** Conceptualization: M.N.D., H.C., S.Oe., S.D.B., Y.R., O.S., and R.Z. Investigation: M.N.D., H.C., M.A., S.Of., J.Pan., M.I., P.Y.-P., M.S., M.Ko., N.G., J.O., G.J., D.S., P.M., A.P., Z.F., A.B., B.U., S.J., E.K., A.Hu., A.Mu., J.J., A.Me., J.L., A.Ha., S.Oe., J.S.-K., S.D.B., Y.R., and R.Z. Methodology: O.S., S.Of., M.Ka., S.D.B., S.Oe., J.Pan., Y.R., N.R., and M.A. Validation: M.A., J.Pan., A.P., S.D.B., M.N.D., and S.Of. Data curation: M.N.D., H.C., M.A., S.Of., N.G., N.R., A.Ha., and J.S.-K. Formal analysis: M.N.D., H.C., M.A., S.Of., S.D.B., A.Mu., N.R., J.J., and J.S.-K. Visualization: M.N.D., H.C., M.I., and M.A. Resources: J.O., J.S.-K., T.H., A.K.-S., M.Ka., S.D.B., O.S., and R.Z. Supervision: M.N.D., H.C., T.H., A.K.-S., S.D.B., Y.R., O.S., and R.Z. Writing—original draft: M.N.D., H.C., and M.A. Writing—review and editing: M.N.D., H.C., M.A., S.Of., J.Pan., M.I., N.G., G.J., J.O., D.S., A.P., N.R., M.P., A.Hu., A.Mu., J.J., A.Ha., J.Pas., S.Oe., J.S.-K., T.H., M.K., S.D.B., Y.R., O.S., and R.Z. Project administration: H.C., S.Oe., S.D.B., O.S., and R.Z. Funding acquisition: H.C., J.Pas., T.H., A.K.-S., M.Ka., S.D.B., Y.R., O.S., and R.Z. **Competing interests:** The authors declare that they have no competing interests. **Data and materials availability:** All data needed to evaluate the conclusions in the paper are present in the paper and/or the Supplementary Materials.

Submitted 17 July 2024
Accepted 11 April 2025
Published 28 May 2025
10.1126/sciadv.adq2348